Thesis for the degree of Licentiate of Engineering
in
Machine and Vehicle Systems

Road vehicle energy demand predictions under uncertain operating conditions

CARL EMVIN

Department of Mechanics and Maritime Sciences
CHALMERS UNIVERSITY OF TECHNOLOGY
Göteborg, Sweden 2026

Road vehicle energy demand predictions under uncertain operating conditions
CARL EMVIN

Thesis of Licentiate of Engineering 2026:03

Department of Mechanics and Maritime Sciences
Chalmers University of Technology
SE–412 96 Göteborg, Sweden
Telephone: +46 (0)31–772 1000

Typeset by the author using LaTeX.

Printed by Chalmers Digital Printing
Göteborg, Sweden 2026

To my love, Hannah.

Road vehicle energy demand predictions under uncertain operating conditions

Carl Emvin
Department of Mechanics and Maritime Sciences
Chalmers University of Technology

Abstract

The push for electric transport has brought new challenges to the vehicle industry, many of which stem from the limited range and long charging time. Consequently, vehicle users who regularly utilize the entire battery during their transport missions may have to endure slow charging speeds, queues, or even immobilization due to battery depletion. Even among some, the mere fear of battery depletion is enough to deter the pursuit of purchasing an electric vehicle. However, with intelligent vehicle functions like range estimators and route-planning algorithms becoming more accurate, users are enabled to make informed choices to address some of these problems. While the literature on routing algorithms is extensive, the focus has merely been on defining the optimization problem and algorithm, often using simple energy consumption models. In contrast, research in range estimation relies on rather complicated energy consumption models, which are often derived from vehicle data. These models do, unfortunately, have poor transferability between different drivers, environmental conditions, and vehicles. A great effort has thus been undertaken to model these effects in isolation, for instance, the study of rolling resistance and air drag. Building on models like those, numerous complex complete vehicle simulation models have been developed with excellent accuracy in controlled environments, but at the cost of being too computationally expensive for in-vehicle use. Additionally, these models seldom quantify uncertainty, a crucial parameter for preventing battery depletion.

To this day, the uncertainty of a range estimate is most commonly inferred from data, sensitivity analyses, or empirical model parameters. Methods relying on data or sensitivity analyses generally impose a constant uncertainty, owing to the estimation methods adopted. In contrast, using a model-based approach, for instance, derived from empirical model parameters, has the advantage of capturing dynamic characteristics that vary between transport missions. Notably, these parameters may not necessarily convey any physical meaning, but instead exist solely as internal elements of a black-box model. In contrast, by adopting a physical model-based approach, variations in energy demand can be derived from exogenous parameters like those obtained from weather, traffic, mission, and road information. This approach aligns precisely with that adopted in this thesis. Specifically, three models are formulated, all aimed at estimating energy

demand uncertainty in the presence of reference-speed perturbations. In two of the models, the reference speed is considered a measurement, permitting the use of the Luenberger observer framework. This novel approach enables the estimator to acknowledge uncertainties from parameters that exert an indirect effect on the energy consumption, typically those affecting the vehicle motion. However, even for these models, merely parameter and model-induced uncertainties were considered, with the major dynamics being known. To assess and quantify the additional uncertainty introduced by certain parameters being undefined, the same transport mission was repeatedly simulated operating under different Gross Combined Weights (GCW). The findings demonstrate that precise knowledge of the GCW is essential for reliable energy demand predictions.

Keywords: energy demand, energy consumption, residual range estimation, motion resistance, observer, stochastic.

Acknowledgments

I have now made the halfway mark on the journey of obtaining the Doctor of Philosophy degree by claiming the licentiate degree. It is with the greatest gratitude that I would like to thank all of you involved who have made this feat possible. Thank you!

Thank you, Professor Fredrik Bruzelius, for your curiosity, knowledge, and support that have guided and inspired me throughout these years. My research and well-being wouldn't have been the same without you. I admire your ability to recognize novelty when it is present. It has been invaluable in my search for the truth of vehicle energy demand.

Thank you, Professor Bengt Jacobsson, for the countless hours you have spent discussing, asking, and testing my knowledge in vehicle energy consumption and related topics. Your meticulous way of breaking down problems has been instrumental to the understanding of others and, frankly, my own research.

Thank you, Doctor Luigi Romano, for introducing me to stochastic models and trusting in my ability to conduct research. I am forever grateful for the time we spent in the office, at conferences, and nowadays over video calls. I admire your attention to details which has improved both my research and writing.

Thank you, PhD student Zhaohui Ge, for being the perfect roommate here at VEAS. You have an astonishing ability to memorize everything that concerns vehicles. I aspire to one day know half of what you know concerning vehicles. I am grateful for all the laughters i have had with you.

Thank you, my project partner and Volvo engineer, Rickard Andersson, for your industry knowledge and ideas. Your interest and trust in me have motivated me to do even more.

Thank you, my project partner and RISE researcher, Pär Johannesson, for your

guidance concerning statistics and stochastic models. Discussing uncertainty and random variables is always a pleasure with you.

Thank you, Sonja Laakso, for making such a hospitable office climate. I have always felt welcomed by you.

Thank you, my beloved Hannah Nilsson, for your love, support, and care. I am forever grateful for the memories we have and continue to create. Your support and care throughout these years have been nothing but instrumental to the progress I've made. You always aspire to make me happy, and you consistently prevail.

Thank you, my childhood family the Emvins: Mother Lisbeth, Father Peter, Brother Albin, and sister Tilda, for your love and care. Your guidance and support started 27 years ago in Trollhättan. I have since then moved to a different city and grown into becoming a researcher, but we still talk regularly, which I appreciate.

Thank you to my friends: Johan Linden and Anton Linden. It is with you that I have had the opportunity of traveling through countries, ideas, and interesting discussions. Johan, thank you for the laughter we shared ever since high school. Anton, thank you for the time we spent together in the Mechanical engineering program at Chalmers and the years after.

Thank you to all my other friends and colleagues who i have made invaluable memories with.

Thesis

This thesis provides additional material complementing the following appended papers:

Paper A **C. Emvin**, L. Romano, F. Bruzelius, B. Jacobson, P. Johannesson, and R. Andersson, "A Kalman-smoother-based known route energy demand predictor for road vehicles," *submitted for journal publication.*

Paper B **C. Emvin**, F. Bruzelius, L. Romano, B. Jacobson, P. Johannesson, and R. Andersson, "A Propulsion Energy Estimator for Road Vehicles," in the 16th International Symposium on Advanced Vehicle Control, 2024, doi: 10.1007/978-3-031-70392-8_45.

Paper C L. Romano, **C. Emvin**, F. Bruzelius, P. Johannesson, R. Andersson, and B. Jacobson, "Stochastic Modeling of Mission Stops and Variable Cargo Weight for Heavy-Duty Trucks," IEEE Vehicle Power and Propulsion Conference, Milan, Italy, 2023, doi: 10.1109/VPPC60535.2023.10403336.

Acronyms

BEV	Battery electric vehicle
BET	Battery electric truck
ICEV	Internal combustion engine vehicle
OC	Operating conditions (previously named operating cycle)
dOC	Deterministic operating conditions
sOC	Stochastic operating conditions
SoC	State of charge
PDF	Probability density function
PMF	Probability mass function
CDF	Cumulative distribution function
EDP	Energy demand prediction (see Definition 2.1)
MCM	Monte Carlo method

Notation

In this thesis, the notation adopted, unless otherwise stated, is as follows: vectors are written in lowercase bold italic font $\boldsymbol{v}$, and matrices in capitalized bold roman font $\mathbf{K}$. The subscript k is reserved for the discrete indexing of the independent variable, whereas continuous functions of time t and space s are written as $f(t)$ and $f(s)$, respectively. Moreover, the subscript i denotes the index of a particle and simulation. Hence, a discrete variable like the longitudinal vehicle speed v_x shall at time k in the simulation i be expressed as $v_{x,\,k,\,i}$.

Table of Contents

Chapter 1

Introduction

1.1 Motivation

Internal combustion engine vehicles (ICEV) are, and have been, dominating sales in most markets due to their flexibility, relatively low total cost of ownership, and acquisition cost. In contrast, electric vehicles have long struggled to compete concerning sales for the same reasons. For medium and heavy-duty trucks, this means that merely 90 thousand or 2% of the worldwide truck sales in 2024 are electric [1]. However, this number is notably different when comparing region by region. In Figure 1.1, the worldwide sales of electric trucks in class medium and heavy-duty are presented over the period 2016-2024. By the numbers, it is evident that the Chinese electric truck market is the largest, and Europe second largest. Still, the share of medium and heavy-duty vehicles sold being electric in the Chinese and European markets is merely 4% and 2% respectively. The consumer is evidently not convinced that an electric vehicle is the best fit for their operation and instead chooses the more flexible option, ICEV. Because with a battery electric truck (BET), the driver has to endure frequent charging stops due to the limited driving range. For the future, advances in battery technology, energy-efficient vehicle design, and the expansion of charging infrastructure are certainly essential to electrification, but they are not the only strategies. Another approach is to render flexibility a redundant feature, which may be accomplished by the introduction of an accurate range estimator and good route planning. With it, questions concerning range may always be answered without ambiguity, thereby having maximum flexibility. By such a range estimator, the space of feasible operations for BETs shall expand as safety margins concerning range can shrink. In [3], the potential of BETs is investigated in Switzerland and Finland, based on the technology available around the year 2018. The study concludes that BETs have much higher commercial potential than what is suggested by the sales numbers. The study also performs a sensitivity analysis of the electrification potential under

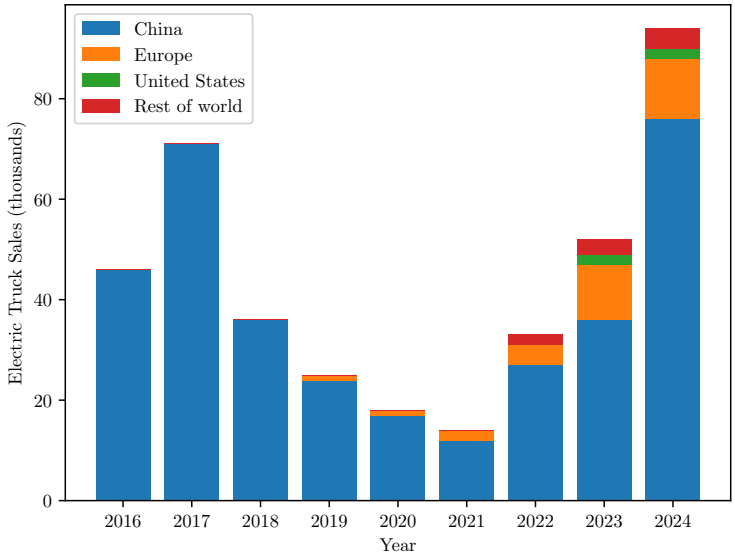

Figure 1.1: The bar plot shows the number of sold electric trucks by region over the period 2016-2024. Each bar is comprised of four slices, with the color representing the sales in each region. The data used in the plot was accessed from [2].

the influence of energy consumption uncertainties. For Switzerland, an increase in energy consumption of 12% corresponds to a decrease in electrification potential of 14%. Observe, the numbers presented in the study correspond to the potential given that the driver has a perfect range estimator; without it, rather big safety margins would have had to be applied to avoid battery depletion. In Finland, the same numbers are significantly smaller due to the generally more demanding transport operations that are not suitable for electric propulsion, for instance, high-capacity transport (HCT) and long-haul operations. Likewise, regions with a limited charging infrastructure will experience difficulties with electrification, as the limited range may render certain operations infeasible.

Thus far, the discussion has revolved merely around the potential of replacing ICEVs with electric vehicles (EVs), having them compete in terms of profitability rather than complement each other. In doing so, one must first realize and acknowledge the benefits associated with each powertrain type, which may include testing new types of transport operations. In the Reel project [4], different types of transport operations were tested using BETs, for instance, urban distribution during nighttime. For conventional vehicles, the sound levels cannot be tolerated at nighttime, but BETs are comparably quiet, demonstrating a potentially new transport operation. Accordingly, the optimal fleet distribution, considering the

benefits of all powertrain types, may be attained from deploying a mixed fleet planning algorithm [5]. The paper adopts a rather simple energy consumption model, here referred to as the specific energy consumption (SEC) model, a common model for these types of studies and algorithms due to its ease and speed of computation. It postulates that energy consumption is proportional to travel distance, by the proportionality constant $\bar{E}$ often measured in $\mathrm{kW\,h\,km^{-1}}$. The paper employs the most rudimentary formulation of the SEC model by assuming a constant proportionality coefficient $\bar{E}$, from which it follows that the energy consumption of route i is given by $E_i = \bar{E}d_i$. Likewise, Paper A also presents a SEC model, but with the distinct difference of modeling time dependence. It revolves around the postulate that two consecutive transport missions have similar average energy consumption: $E_i = \bar{E}_{i-1}d_i$. Owing to its design, variations in energy consumption are difficult to account for, as the calculation relies exclusively on previously elapsed information rather than parameters of the ongoing transport mission.

In a European Commission study, a big set of petrol cars of category "Large car" have had their fuel consumption and distance traveled recorded by an on-board fuel consumption monitoring (OBFCM) device [6]. The data was collected from approximately one-fifth of all newly registered passenger vehicles in Europe in 2021. For these vehicles, the yearly SEC value is presented in a histogram, Figure 1.2, highlighting the differences in energy consumption across vehicles and vehicle usage. The figure illustrates the extent of variation that can arise solely from differences in operating conditions and driver behavior, as the vehicles examined are largely comparable, owing to their similar kerb weights. Notably, working with heavy vehicles shall generate significantly larger variations as the gross combined weight can be a fourfold larger, comparing a loaded to a tare vehicle combination.

Having outlined several technological pathways through which the transport sector may be electrified, it is equally important to consider the underlying motivation for pursuing this transition. In [7], it is stated that a two-degree increase in average temperature would put half of Africa's population at risk of undernourishment. In addition, multiple studies manifest that the world must make a change in trajectory concerning CO_2 emissions to avoid causing irreversible damage to certain ecosystems. To this day, 194 states have signed the Paris agreement, confirming the ongoing climate change and sharing the ambition of never exceeding a two-degree increase in average temperature compared to the preindustrial era. The treaty stipulates that each party is encouraged to file its own national adaptation plans aiming to reach the climate goal. In Europe, these plans are realized by, for instance, CO_2 emission standards [8]. When it comes to greenhouse gases, three dominating sectors can be identified, including: Electricity and heat processes, industry, and transportation, whereas a large portion of the emissions

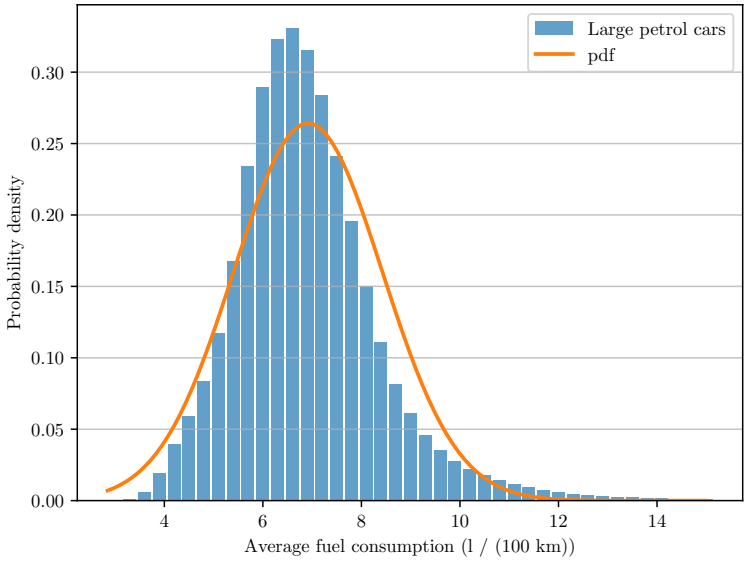

Figure 1.2: The figure shows the variation in average fuel consumption for large petrol passenger vehicles based on a large set of real-world measurements, attained from [6].

from transportation is due to road transportation, as can be seen in Figure 1.3. Therefore, significant regulations are put in place by the EU regulation, demanding emission reductions of 30% for newly sold heavy vehicles. This reduction is compared against reference CO_2 emissions based on monitoring data from the period 1st of July 2019 to 30th of June 2021. To remain competitive within the vehicle industry, one must therefore find a solution that complies with these goals and regulations.

To quantify, predict, and analyze CO2 emissions from the transportation sector, there have been numerous initiatives, with an important one being the Vehicle Energy Consumption calculation Tool (VECTO) developed by the European Commission. Based on the declared values it produces, customers and legislators can make informed choices towards more sustainable means of transportation. The model has demonstrated good overall accuracy, although it struggles to reproduce variations observed in real operations, owing to the scarcity of reference missions. A further concern regards the risk of consolidating old technical solutions, arising from the reliance on simulation rather than measurements. Most importantly, it shall not be used as a range estimator, since the reference missions do not convey information about the ongoing transport mission. In reality, the actual energy consumption of vehicles depends on vehicle-use and does therefore not always follow the declared values, which were for passenger vehicles concluded

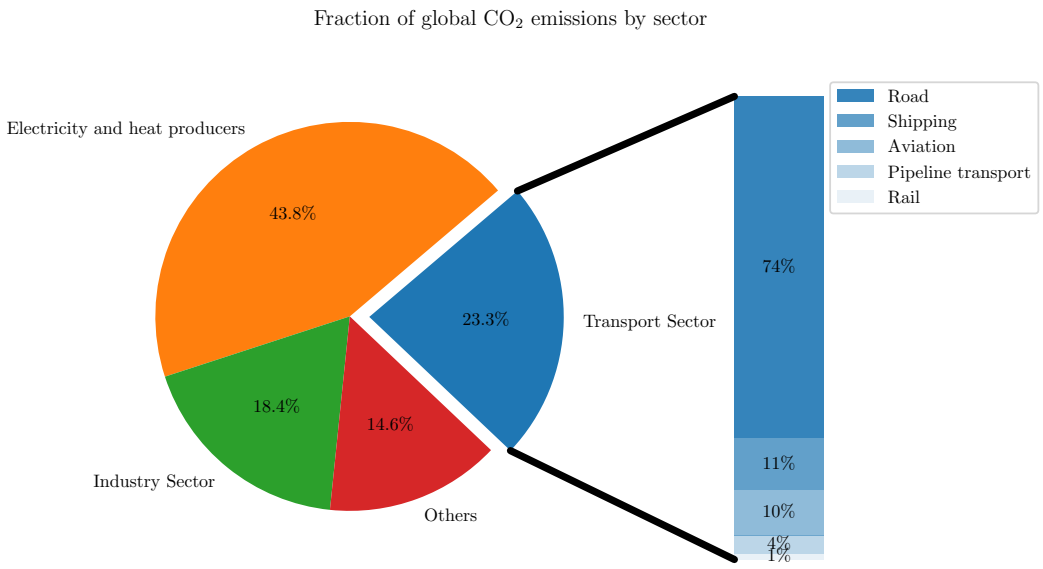

Figure 1.3: The transport sector is responsible of approximately $\frac{1}{4}$ of all CO_2 emissions, of which road transport account for $\frac{3}{4}$.

in a recent report by the EU commission [6]. In the report, the average fuel consumption of petrol cars was found to be 20% higher than what was estimated from the VECTO software. The difference was, amongst others, attributed to the fact that real vehicle operation has a larger variation in operating conditions than that of the driving cycles.

Building on what has been stated above, the need for accurate energy consumption models, range estimators, and simulation software cannot be understated. With accurate meaning, both concerning average error, as was discussed in relation to VECTO, but also in terms of variation, discussed in relation to the OBFCM data. The thesis will therefore provide algorithms, concerns, discussions, and results focusing on the core aspects related to energy consumption and its variation. In particular, the thesis will concentrate on energy demand, Definition 2.1, which serves as a powertrain-agnostic definition of energy consumption.

1.2 Research questions

This thesis addresses three research questions, focusing on energy demand prediction (EDP) and its uncertainty. The first question concerns the best practice of EDP, the second pertains to methods used in EDP uncertainty estimation, and the third addresses the effect of stochastic mission characteristics on the EDP

accuracy.

I. **Modeling:** Which are the methods, assumptions, and models that comprise an EDP algorithm?

   The question highlights the many assumptions adopted by physics-based EDP algorithms. Depending on the problem formulation and objective, the appropriate model, method, and thereby assumptions may differ, which must be identified.

II. **Uncertainty:** How can the EDP uncertainty be estimated, and what shall be accounted for?

   The question concerns the benefits of deriving the EDP uncertainty from exogenous parameters and how such a framework may manifest itself. The specific algorithm of choice is here secondary, and focus is rather on how to interpret each parameter and its role in the EDP algorithm.

III. **Absence of observations:** How shall EDPs be conducted in the absence of observations, and how does it affect the EDP uncertainty?

   This research question addresses the challenges associated with the absence of observations, in particular vehicle weight, when performing EDPs. These challenges shall be quantified and studied such that all EDP algorithms may benefit from the conclusions.

1.3 Scientific contributions

This thesis delivers a compilation of EDP algorithms tailored to each problem, outlined in every Chapter. In Paper A, a novel method for estimating the energy demand using a cubature Rauch-Tung-Striebel smoother was developed. It was demonstrated that an observable estimator can be attained from interpreting the reference speed as a measurement. Using merely exogenous parameters, the energy demand and its uncertainty were obtained, showing promising results. In paper B, an analytical solution of the truncation error was derived. It emphasizes the importance of compliance in the EDP algorithm and the effect certain pedal arbitration functions may have in combination with noisy measurements. The error was shown to be the largest at high-speed free-rolling conditions. In Paper C, a stochastic model of the cargo weight and mission stops was developed. The cargo weight was modeled by assuming the vehicle only exhibits four distinct modes, and that the transitions between those obey the Markov property.

1.4 Limitations

The thesis presents methods for conducting EDPs, which do not directly address the same challenges as an energy consumption predictor or a residual range estimator does. These models capture the consumed energy due to motion resistances and braking, but neglect many other important factors related to energy consumption. For instance, the algorithms presented do not capture the dynamic behavior, limitations, and efficiencies of a powertrain, as the energy demand is calculated at the wheel rather than in the energy storage system.

Another aspect is the simplifications and assumptions employed throughout the thesis. In general, more complex vehicle characteristics and dynamic effects are often omitted to enable certain frameworks or to obtain analytical expressions for the uncertainty. In those instances, the impact and validity of each simplification are discussed.

Lastly, assessing the performance of different EDP algorithms is rather difficult as it is largely determined by the availability of information, the measurement quality, the transport mission, and the test vehicle itself. One shall therefore be careful when comparing the numerical results presented in this thesis with those in other publications. Inductive conclusions may certainly be drawn, provided that the operation and setup are comparable, although deductive conclusions are preferred in this thesis.

1.5 Outline

The purpose of the thesis is to further explain, exemplify, and discuss the methods and models developed in the appended papers. Analogously, the methods developed in the thesis are, in general, simplifications of those in the attached papers, but characterized by the same ideas and novelty. Large parts of the thesis shall therefore be understandable to someone with an engineering background. However, for certain parts of the thesis, further knowledge in estimation theory and stochastic models may be beneficial. In particular, the reader is advised to familiarize themselves with nonlinear acausal observers [9] and common stochastic models [10] to understand the contents of Chapter 3 and 4. These concepts are briefly explained in the thesis, but without all the details.

The thesis is organized as follows: Chapter 2 is devoted to the underlying equations that describe longitudinal motion. It involves modeling the driver and the vehicle, with the primary focus on motion resistances and traction force. Throughout the Chapter, each step is discussed concerning the simplifications and assumptions made and their effect on the EDP accuracy. It is also here that the SEC and inverse dynamic model are introduced and discussed. The

purpose of Chapter 3 is to present, describe, and establish the observer-based EDP model that was developed in Paper B through the introduction of two new, but related, models with similar properties. It aspires to serve as a complement to the paper, rather than a repetition, ending with a small summary of the model itself. Throughout the Chapter, the discussions revolve around EDP uncertainty and its effect on the mean energy demand. Importantly, the uncertainties considered in this Chapter originate from model assumptions and measurement inaccuracies, which manifest themselves as noise. In contrast, Chapter 4 presents methods for estimating the uncertainty in the absence of measurements, specifically the cargo weight. There, a simple simulation experiment is conducted to understand the importance of accurate cargo weight measurements in EDPs. Finally, the methods, results, and discussions presented are all discussed in relation to the research questions in Chapter 5.

Chapter 2

Energy demand prediction

In this Chapter, the fundamental definitions and methods utilized in EDP algorithms are introduced, including motion resistances and generic system architectures. These concepts are introduced with an emphasis on physical modeling, omitting fully empirical algorithms. Certainly, parts of the physical system description require the adoption of semi-physical models, as these phenomena aren't yet fully understood; for instance, rolling resistance. In addition, the models, parameters, and complete system description presented in this Chapter assume all inputs and states are deterministic, neglecting the influence of higher-order moments. In the coming Chapters, the randomness of certain variables is acknowledged, and their effects on the average energy consumption are studied. Without further proof for now, randomness in input parameters typically increases average energy consumption compared to using averaged variables, since all relevant functions involved are convex. Under these considerations, the results from this Chapter may be interpreted as lower bounds to the real energy demand, assuming the real parameters exhibit randomness.

Before delving into the details of energy demand, it must first be defined to avoid confusion. By Definition 2.1, the energy demand is the positive mechanical work conducted at the contact patch in the driven axle. With this definition, longitudinal driver modeling becomes crucial, as braking is seen as a power loss. In contrast, the energy dissipation due to motion resistances, Definition 2.2, assumes ideal brake regeneration in all axles, which makes the measure less sensitive to the driver model. They are therefore rarely the same, except for the special case in which no brake torque is applied. Notably, both measures are by definition independent of the powertrain, as the mechanical work is studied before the powertrain, but depend on the vehicle's characteristic parameters: rolling resistance and drag coefficient. Therefore, none of these definitions represent the actual energy consumption, as powertrain losses and auxiliaries aren't modeled, but they both provide a good foundation for such studies. To facilitate them, the EDP

model must provide the effort and flow variables, force and speed, or torque and rotational speed, so that the powertrain efficiencies can be attained from a consumption map or using a component-based structure, e.g [11] and [12]. While not directly deployed in this thesis, publications and references focusing on powertrain efficiencies and motion resistances are certainly relevant for contextualization and perhaps evaluation.

Definition 2.1 (Energy demand)**.** Energy demand E is defined as the positive mechanical work conducted in the contact patch of the driven axle,

$$E(s) = \int_0^s F_{\mathrm{p}}(s')\,\mathrm{d}s'. \tag{2.1}$$

In equation (2.1), the propulsion force F_{p} is the traction force F_{t} component that is codirectional to the vehicle motion, defined as:

$$F_{\mathrm{p}} = \begin{cases} F_{\mathrm{t}}, & \text{if } F_{\mathrm{t}} \geq 0 \\ 0, & \text{otherwise.} \end{cases} \tag{2.2}$$

Definition 2.2 (Energy dissipation due to motion resistance)**.** The energy dissipated due to motion resistances E_{mr} is defined as the mechanical work conducted in the contact patch of the driven axle,

$$E(s) = \int_0^s F_{\mathrm{t}}(s')\,\mathrm{d}s'. \tag{2.3}$$

In light of this, the generic EDP algorithm can now be introduced, an architectural model that represents all physics-based and most empirical EDP algorithms, consisting of three modules: the *environment*, *driver*, and *vehicle*. Most models consist of these modules, although not always explicitly mentioned, for instance, a regression model with the regressor: vehicle mass, estimates the rolling resistance coefficient. Even history-based prediction algorithms use this structure by imposing that the driver, environment, and vehicle parameters of the future will be similar to those of the past. In other words, the architectural model discussed is the underlying plant model that EDP algorithms wish to estimate. In Figure 2.1, a schematic representation of the model is presented, where the blue solid arrows indicate information sharing between the three modules, and the green dotted arrows represent EDP dependencies. Observe that the driver cannot affect the environment in the generic EDP algorithm, signified by the unidirectional

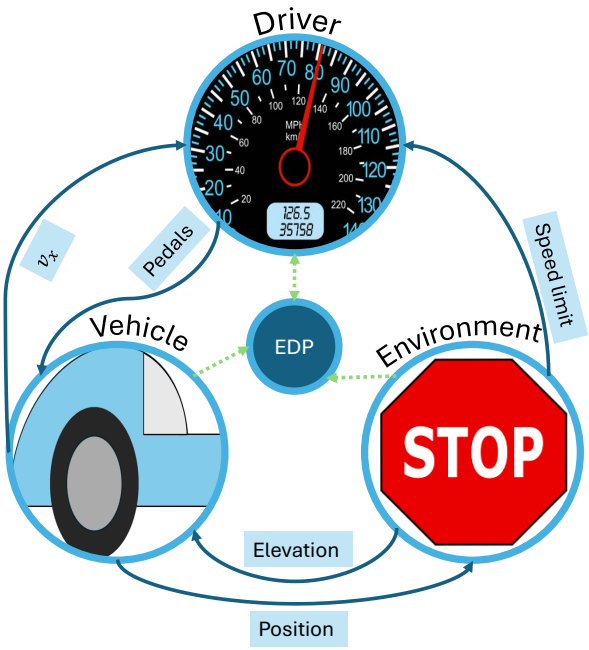

Figure 2.1: The figure describes a generic energy demand predictor with blue arrows indicating transfer of information and green arrows indicating dependencies.

information flow. It follows from the assumption that the route is known and determined, rendering the environment independent of the driver. This is a crucial assumption for most EDP algorithms, as it enables the use of road, weather, and traffic information. In reality, this assumption may not always hold, as human drivers can affect the environment through the choice of route, time of start, and the mission's characteristics, sometimes even after the mission has been initiated. Obvious examples include missed exits, wrong turns, or the decision to change transport mission. Another aspect to consider is the absence of information resulting from inadequate communication between the driver and the vehicle. This problem is partially handled in Chapter 4, in which the cargo weight is unknown to the vehicle. Likewise, there are publications of EDP algorithms in which the route isn't specified, for instance [13]. For this type of problem, the customary solution is to present the reachable destinations on a 2d map. To produce such a solution, one must assume that the driver has a course; otherwise, the area doesn't mean much. Taking this argument to the absurdum, the vehicle may deplete its whole energy storage system by simply circulating in a roundabout or by idling. But for the time being, the environment is considered known to the vehicle and the EDP algorithm. Another aspect to consider concerns the randomness of parameters and states used in EDP algorithms. In practice, many of the parameters used have significant uncertainty, with some of the adverse effects being covered

in Paper B. But to avoid confusion, merely deterministic representations are presented in this Chapter, and the effects of randomness are instead covered in later parts of the thesis.

2.1 Driver

A longitudinal driver controls the pedal angles, often based on external stimuli. For instance, an adaptive cruise controller determines the pedal angles in response to the tracking error, that is, the distance to and the speed of the lead vehicle [14]. The same principles and model may be applied in the context of EDPs, denoted as the *operational driver*. Here, the lead vehicle are strictly virtual, often manifested as a reference speed that the operational driver shall follow. To produce the reference speed, it is often required to have a *tactical driver*, with the sole purpose of describing the tracking error of the lead vehicle. This type of driver is covered in detail in Section 2.1.1, where vehicle speed-relevant information from road data, such as the curvature and the distance to the next stop sign, is used to produce a reference speed. Building on the two driver modules, the complete driver can

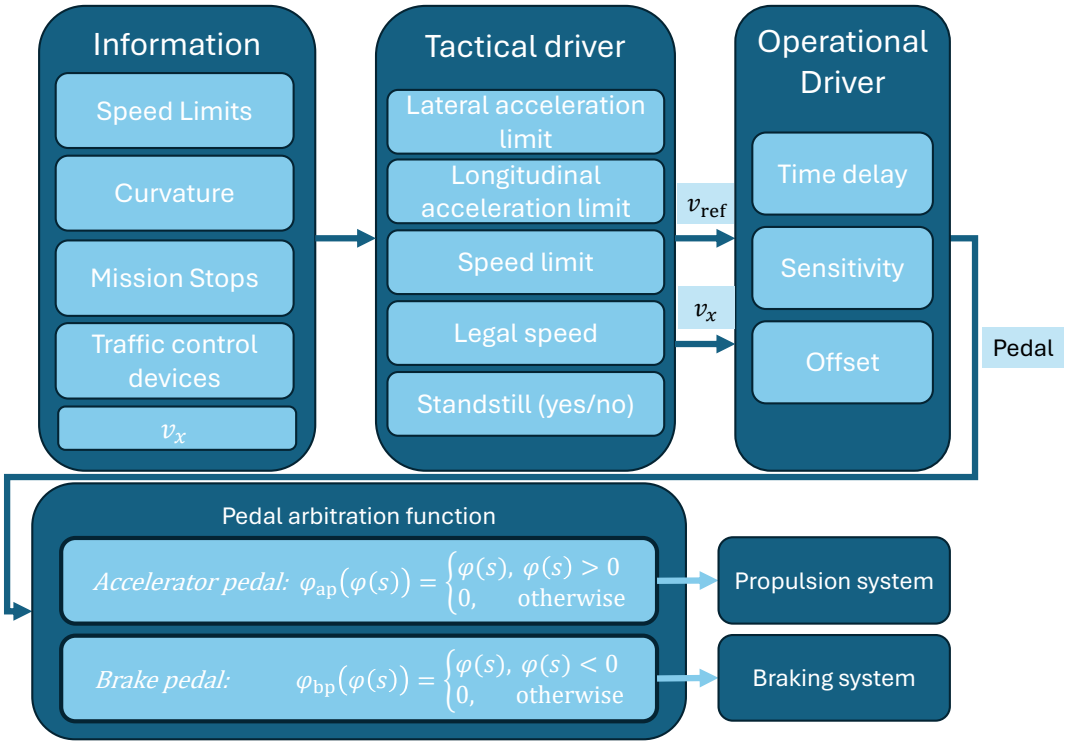

Figure 2.2: A flow diagram of a longitudinal driver that transforms external stimuli to a set of accelerator and braking pedal angles.

now be introduced in Figure 2.2, which is characterized by the unidirectional flow of information. After the operational driver, the pedal angle passes through a pedal arbitration function that determines the distribution between the brake and accelerator pedal. Throughout this thesis, the pedal arbitration function defined in Figure 2.2 is adopted, which assumes mutually exclusive pedals, meaning both pedals cannot be used simultaneously.

2.1.1 Tactical driver

The tactical driver's primary purpose is to establish a reference speed, which can be achieved through various means. In [15], a reference speed based on free-flow speed measurements, attained from road maps providers, is used. In contrast, [16] derives a probabilistic model from repetitive simulations of a high-fidelity model under different traffic conditions. Albeit different, both papers adopt a mean segment speed approach, considering each segment to have three characteristic speeds: the start, end, and mean speed. To smooth out the discontinuities, each consecutive road segment is patched together by adopting the constant acceleration model, i.e., the driver accelerates or decelerates over the junction until the new mean segment speed is attained. An even simpler alternative is to increase the length of segments, such that the whole transport mission is explained by one road segment, which reduces the driver to merely using one reference speed for the whole transport mission. The approach is appealing, but lacks the fundamental ability to represent stop-and-go behavior common in urban environments. Although this example is extreme, the use of mean segment speed inherently hides high-frequency behavior that may, for certain transport operations, have a significant impact on energy consumption. For instance, segments containing stop signs may have a low mean speed, but large speed variations, as a human driver will reduce the vehicle speed to zero before the sign and then accelerate. It is therefore important when working with these mean speed models to understand how they have been produced and what the energy demand-related consequences are. Another approach is taken in Paper A, where the reference speed is described entirely by road and mission information. There is certainly potential for complementing with other sources of information, including traffic and weather, but it was not considered in that study. Nevertheless, this type of driver can capture stop-and-go behavior, owing to the information used. Its functionality is for the same reason, independent of vehicle log data, permitting it to be used in virtual environments constructed of roads that do not necessarily exist, making this driver particularly appealing in virtual testing.

Specifically, the tactical driver used in this thesis produces a reference speed v_{d} based on sensory information, including legal speed (l), curvature (c), mission stops (m), and traffic control devices (t), with the latter being comprised of traffic

signals, stop signs, yield signs, and pedestrian crossings, i.e all the zero speed observations. The information is first passed through the direct module, which assesses the current situation, and subsequently through the look-ahead module to account for the future, essentially limiting the longitudinal acceleration. In the first pass, the direct driver module,

$$v_{\mathrm{d}}^{-} = \min(v_{\mathrm{l}}^{-}, v_{\mathrm{c}}^{-}, v_{\mathrm{t}}^{-}, v_{\mathrm{m}}^{-}), \tag{2.4}$$

generates a reference speed equal to the maximum speed permitted, obeying four speed constraints all derived from the sensory information: legal speed, curvature, traffic control devices, and mission stops. Here, the legal speed constraint, v_{l}^{-}, corresponds to the legally permitted speed for the specific vehicle combination, i.e., the maximum speed allowed, obeying the speed limit and the combination's maximum legal speed. The second speed constraint concerns the road curvature, specifically, the lateral acceleration generated during steady-state driving in a curve. It follows that the lateral acceleration for a point mass is the product of the squared longitudinal vehicle velocity and the curvature C, expressed as the inverse of the curve radius. Hence, by defining a lateral acceleration limit $a_{y\mathrm{l}}$, the curvature-related speed constraint can be expressed as:

$$v_{\mathrm{c}}^{-} = \sqrt{\frac{a_{y\mathrm{l}}}{C}}. \tag{2.5}$$

The third speed constraint regards traffic control devices and their influence on the reference speed. With limited presence, they seldom influence the driver, but when they do, it can mathematically be described by the equation:

$$v_{\mathrm{t}}^{-} = \begin{cases} 0, & \text{if traffic control device} \\ \infty, & \text{otherwise.} \end{cases} \tag{2.6}$$

Likewise, the mission stop-related speed constraint, $v_{\mathrm{m}}^{-} = 0$, is only active under certain circumstances, that is, during driver rest and cargo change. To assure a comfortable ride, the look-ahead driver module adjusts the reference speed of the present k and imminent future $k + n$ to comply with a longitudinal acceleration limit $a_{x\mathrm{l}}$. This may be satisfied through the use of the kinematic relations,

$$v_{\mathrm{d},\,k}^{+} = \sqrt{2n\Delta s a_{x\mathrm{l}} + (v_{\mathrm{d},\,k+n}^{-})^2}, \qquad v_{\mathrm{d},\,k+n}^{+} = \sqrt{2n\Delta s a_{x\mathrm{l}} + (v_{\mathrm{d},\,k}^{-})^2} \tag{2.7}$$

where the first equation $v_{\mathrm{d},\,k}^{+}$ determines the maximum speed permitted in k given a certain speed in $k + n$, and the second $v_{\mathrm{d},\,k+n}^{+}$ specifies the maximum speed in $k + n$ given a speed in n. That is, the first concerns decelerations and the second accelerations. Apart from the already introduced quantities, the equation also contains the sample distance Δs and the unit step $n \in \mathbb{N}$.

2.1.2 Operational driver

In this thesis, the operational driver is modeled as a simple P-regulator,

$$\varphi(s) = K_{\mathrm{p}}(v_{\mathrm{d}}^{+}(s) - v_x(s)), \tag{2.8}$$

where the proportional gain $K_{\mathrm{p}} \in (0, \infty)$. This type of controller is often adopted by adaptive cruise controllers, as was elaborated earlier, with the focus on controlling the distance or time to the lead vehicle. For EDPs, there is no risk of colliding with the virtual lead vehicle, rendering distance an obsolete control variable; however, the speed error is still relevant. After the pedal angle has been calculated, there is still rather much to consider before a wheel torque can be attained, for instance, the modeling of the actuator, transmission, and driveshaft. These components generally have power losses and contribute to time delays, both of which are neglected when conducting EDPs, permitting the assumption that $F_{\mathrm{t}}(s) \propto \varphi(s)$. Concerning energy consumption, the power losses are certainly relevant and should be modeled, but the time delays can most often be neglected, even in such studies.

2.2 Vehicle

The vehicle module in a complete vehicle simulation generally consists of models for the powertrain, energy storage system, and the governing equation for longitudinal vehicle motion. In contrast, the energy demand merely considers the longitudinal balance equation, following from Definition 2.1. Certainly, the powertrain is important for transient power analysis, as the stiffness of the driveshaft, the response time of the fuel pumps, and more set the characteristics of the power output. However, for longer driving distances, these high-frequency effects are not as prominent, and the focus is instead on motion resistances and driver behavior. Notably, the attached papers and parts of this thesis present results in which EDP algorithms are compared with real vehicle logged energy consumption, which is measured at the crankshaft. To make the comparison fair, a constant drivetrain efficiency is adopted for the EDP algorithm. For these results, possible improvements in accuracy shall be expected by using more intricate drivetrain models.

The vehicle log data used throughout this thesis comes from a rigid 8×2 heavy vehicle with the possibility of attaching a small trailer, with its forces presented in Figure 2.3. It operates under air drag F_{ad}, rolling resistance F_{rr}, hill climbing force F_{hc}, and is controlled through the traction force F_{t}. These forces represent the majority of the motion resistance that the vehicle must overcome, neglecting momentary losses from tyre scrubbing, cornering resistance, and suspension losses, owing to their insignificant contributions to energy demand over

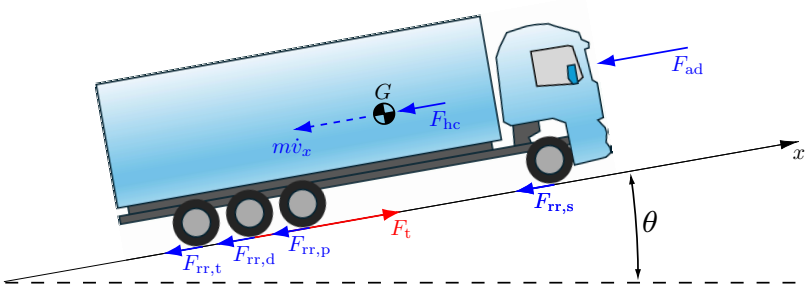

Figure 2.3: A free body diagram of a 8×2 rigid heavy vehicle. The forces acting on the vehicle is air drag F_{ad}, hillclimbing force F_{hc}, traction force F_{t}, and rolling resistance force F_{rr} on each of the axles: tag (t), drive (d), pusher (p), and steer (s).

an entire transport mission. In [17], suspension losses were studied for a set of different road classes, characterized by their power spectral density. The study showed that the suspension loss on a type A road with a bus was no more than 100 W, but significant during their Belgian road test, amounting to 6.7 kW. In [18], cornering resistance as a function of curvature and vehicle speed was investigated. It was found that for a test scenario, the cornering resistance was responsible of 7.5 % of the total energy consumption, with the majority of the cornering resistance contribution to the energy demand occurring in urban traffic with tight turns and low vehicle speed. Likewise, it was discussed that for long-haul operation, in which the curvatures encountered are small, a reduced impact from cornering resistance shall be expected. Hence, the cornering resistance and suspension losses, under specific scenarios, significantly contribute to the energy demand, but in others have a marginal effect. In addition, the estimation of suspension losses poses practical implications, requiring the power spectral density of the road, which ought to be acknowledged. Concerning tyre scrubbing, the author found no publications specifically addressing its energy losses, but the impact is expected to be smaller than that of cornering resistance. Although these three forces are neglected in this thesis, they should all be borne in mind when studying relevant vehicle applications. For instance, it is conceivable that urban bus and truck operations may experience large suspension and cornering losses, as their operation may involve rough roads and frequent tight curves.

Apart from this, the primary benefit of the complete vehicle model regards the possibility of describing individual wheel forces, allowing for a more accurate rolling resistance estimation by incorporating effects associated with weight distribution, lifted tag axle, and drive torque. However, this information is mostly unavailable to the EDP algorithms presented in this thesis. Therefore, an even

simpler model is used, the uni-wheel vehicle, presented in Figure 2.4.

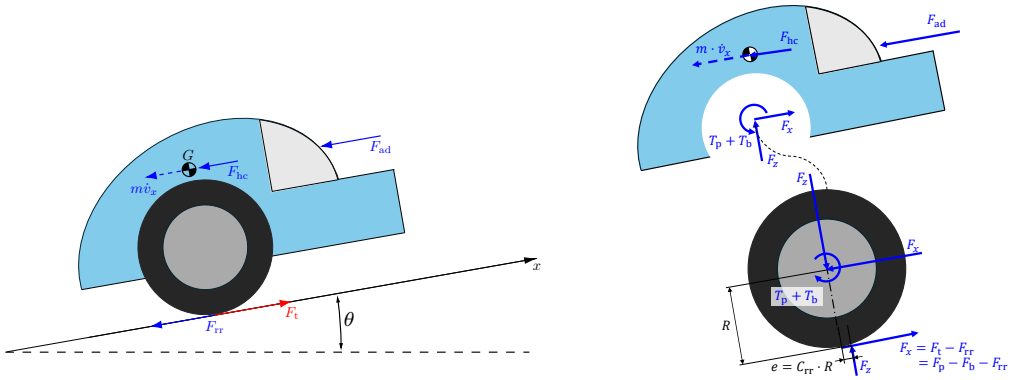

Figure 2.4: A free body diagram of a uni-wheel vehicle. The forces acting on the vehicle is air drag F_{ad}, hillclimbing force F_{hc}, traction force F_t, and rolling resistance force F_{rr}.

Compared to the complete vehicle, the uni-wheel vehicle is a much simpler model, but a better representation of the EDP algorithms used throughout this thesis. Building on the free body diagram in Figure 2.4, the longitudinal balance equation,

$$\frac{\mathrm{d}}{\mathrm{d}t}(mv_x) = F_t - (F_{ad} + F_{rr} + F_{hc}) = F_t - F_{mr}, \tag{2.9}$$

can be formed. As for how equation (2.9) is written, changes in the cargo weight are correctly accounted for, albeit unnecessarily complicated. Provided that the loss of cargo, rainfall, and fuel consumption amount to a small change in mass during travel, the term $v_x\dot{m}$ may be neglected. Clearly, the major changes in gross combined weight occur at a standstill, by loading and unloading the cargo, in which case the longitudinal velocity is zero and cancels the term completely. With this simplification, one may form the governing equation for longitudinal motion,

$$\frac{\mathrm{d}}{\mathrm{d}s}v_x = \frac{F_t - F_{mr}}{mv_x}, \tag{2.10}$$

with position s as the independent variable. Here, position refers to the distance traveled along a three-dimensional path, i.e, the arc length of the path. For certain applications, e.g. Paper A, it may be beneficial to write the equation in this form, as road information and hence also the tactical driver is often provided with distance as the independent variable.

That said, with the traction force defined by the operational driver and the governing equation (2.10) introduced, the only remaining quantity to describe is the motion resistance F_{mr}. It is comprised of the air drag F_{rr}, rolling resistance F_{rr}, and hill climbing force F_{hc}, also called grade resistance. Together, they make

up the resistive forces acting in the opposite direction of travel, except for the hill-climbing force, whose sign depends on the slope's sign. In the coming paragraphs, a set of models for each of the resistive forces is introduced, all of which will be used throughout the thesis, starting with the rolling resistance. The phenomena may partially be explained by the compression-decompression cycle of the tyre rubber as the wheel rolls on the ground, called rubber hysteresis. This effect is responsible for the major part of the rolling resistance, typically around $80-95\%$ of the total rolling resistance of a free rolling wheel [19]. In addition, driven wheels will have the rubber compressed in the longitudinal direction when propelling and braking. Likewise, a cornering vehicle will impose compression in the lateral direction, called cornering resistance. However, these effects are rather small compared to the hysteresis of a free rolling tyre and is therfore neglected in this thesis. In particular, the free rolling resistance,

$$F_{\mathrm{rr}} = C_{\mathrm{rr}} m g, \tag{2.11}$$

is the force opposing vehicle motion resulting from the wheel moment caused by hysteresis in the tire rubber, commonly modeled as linearly proportional to vehicle weight through the rolling resistance coefficient C_{rr}. In [20], this coefficient is shown to directly depend on tire temperature T_{t}, and tire inflation pressure. The effect was also identified in [21], in which the tire temperature-dependent rolling resistance coefficient is presented,

$$C_{\mathrm{rr}} = c_1 + (c_2 - c_1)\mathrm{e}^{-\frac{1}{\lambda}T_{\mathrm{t}}}. \tag{2.12}$$

In (2.12), the constant c_1 is the rolling resistance coefficient at high speeds, c_2 is the rolling resistance coefficient at low temperatures ($T_{\mathrm{t}} = 0\ ^{\circ}C$), and λ is a decay parameter. Notably, the tire temperature T_{t} is the lumped approximation of the distributed state, which has been adopted to simplify the problem. Accordingly, the tire temperature has shown to converge towards a stable temperature T_{t}^* if the operating conditions remain constant, satisfying the ordinary differential equation (ODE),

$$\frac{\mathrm{d}T_{\mathrm{t}}}{\mathrm{d}s} = \frac{T_{\mathrm{t}} - T_{\mathrm{t}}^*}{\tau v_x}, \tag{2.13}$$

where τ represents the relaxation time. The model described here is rather complicated to use, and its parameters can only be identified if certain information is available. For that reason, many EDP algorithms adopt a simpler model, assuming constant rolling resistance coefficient.

Concerning the air drag force, Paper A and B both adopt the model described in [22]:

$$F_{\mathrm{ad}} = \frac{1}{2}\rho A_{\mathrm{p}} C_{\mathrm{D}} \|\boldsymbol{v}_{\mathrm{r}}\|_2^2. \tag{2.14}$$

It follows that the air drag experienced by the vehicle is a function of the sum of vehicle speed $\boldsymbol{v}_\mathrm{v}$ and the wind speed $\boldsymbol{v}_\mathrm{w}$, denoted the relative vehicle speed $\boldsymbol{v}_\mathrm{r} = \boldsymbol{v}_\mathrm{w} - \boldsymbol{v}_\mathrm{v}$. These velocities are all vectors represented in the global coordinate system, allowing for easier manipulation of equations later. Returning to equation (2.14), the air density can be estimated from the the ideal gas law,

$$\rho = \frac{p_\mathrm{d}}{R_\mathrm{d} T_\mathrm{a}} + \frac{p_\mathrm{v}}{R_\mathrm{v} T_\mathrm{a}}, \tag{2.15}$$

where T_a is the ambient temperature, p_d the dry air pressure, R_d is the dry air specific gas constant, p_v the vapor pressure, and R_v is the vapor specific gas constant. Furthermore, the projected area,

$$A_\mathrm{p} = A_\mathrm{f} \cos \varphi_\mathrm{aa} + (A_\mathrm{rs} + A_\mathrm{ts}) \sin |\varphi_\mathrm{aa}|, \tag{2.16}$$

of a rigid truck can be described by the side area A_rs, the trailer side area A_ts, the front area A_f, and the attack angle φ_aa, which is the angle between the relative vehicle velocity and the longitudinal vehicle axis,

$$\varphi_\mathrm{aa} = \arccos \frac{-\boldsymbol{v}_\mathrm{v} \cdot \boldsymbol{v}_\mathrm{r}}{\|\boldsymbol{v}_\mathrm{v}\|_2 \|\boldsymbol{v}_\mathrm{r}\|_2}. \tag{2.17}$$

Finally, the air drag coefficient,

$$C_\mathrm{D} = C_0 \cos^2 \varphi_\mathrm{aa}, \tag{2.18}$$

is characterized by the nominal air drag coefficient C_0 and the attack angle. Altogether, it comprises the wind-dependent air drag model that has been used throughout this thesis. By assuming a wind velocity of $\boldsymbol{v}_\mathrm{w} := 0$, the equations simplifies to the more conventional model:

$$F_\mathrm{ad} = \frac{1}{2} \rho A_\mathrm{f} C_\mathrm{D} v_x^2, \tag{2.19}$$

which is commonly employed by EDP algorithms, and similarly in certain Sections of this thesis.

The last motion resistance, the hill climbing force F_hc, also known as grade resistance, is the gravitational force component parallel to the road slope θ,

$$F_\mathrm{hc} = mg \sin \theta. \tag{2.20}$$

2.3 Inverse dynamic simulation

In the previous two Sections, the driver and vehicle that comprise a dynamic simulation model were explained in detail. Accordingly, its solution can be obtained

from solving the initial value problem, often referred to as a forward simulation. In this Section, another method of computing the traction force is presented, the inverse dynamic simulation model, often referred to as backwards simulation. The model in its most basic form,

$$F := ma, \tag{2.21}$$

is often used in vehicle EDPs and in other fields such as robotics owing to its simplicity. Fundamentally, this approach finds the forces required to realize a prescribed trajectory by regarding all states as known quantities. Doing so, the governing equation becomes algebraic, and the force F can be solved instantaneously. For EDP models with only one driven axle, the set of solutions is unique, which makes this model appealing. In Paper B, the inverse dynamic model was used to derive the energy demand using information that is typically not available to an EDP algorithm, including speedometer and odometer measurements, to estimate the acceleration profile using a constrained Kalman filter. As opposed to the model presented in Figure 2.1, the inverse dynamic model is characterized by the open-loop structure, highlighted in Figure 2.5. To avoid repetition, the equations comprising the vehicle are not stated, but the reader is instead referred to those outlined in Section 2.2, considering motion resistances. Instead, the focus revolves around explaining the driver, or more correctly stated, the trajectory generator.

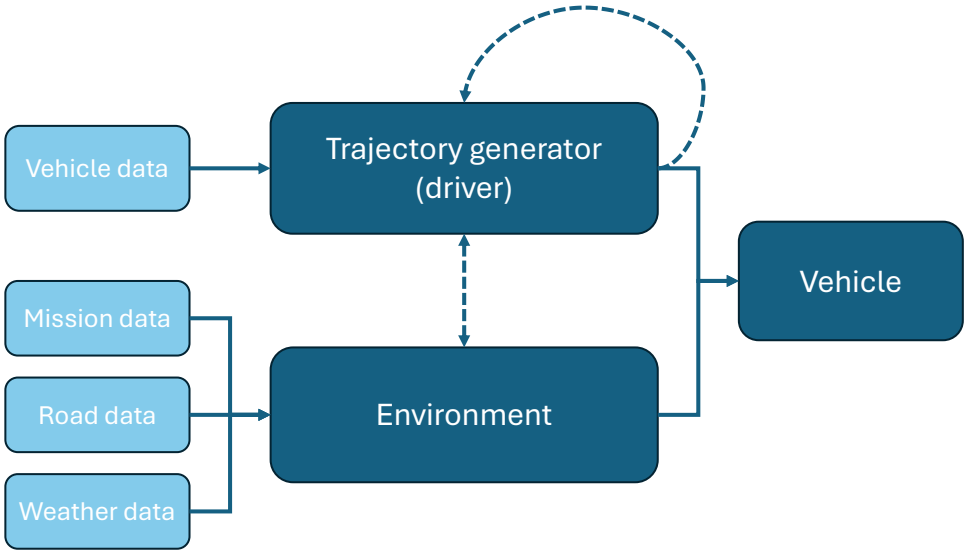

Figure 2.5: A schematic representation of an inverse-dynamic simulation model, with solid lines indicating necessary information flow and dashed lines indicating potential information flow. Depending on the model, the dashed lines may or may not be present, as they are not vital but desirable.

2.3.1 Trajectory generators

A large array of different trajectory generation algorithms can be found in the literature, many of which belong to the research domain of driving cycles. All of these methods produce a trajectory that the vehicle is supposed to follow, but differences in the problem formulation drastically limit the set of possible methods. For instance, the Worldwide Harmonised Light-duty Test Cycle (WLTC) [23] and Vehicle Energy Consumption Calculation TOol (VECTO) [24] are or contain driving cycles used to quantify fuel consumption and emissions for certain vehicles on a macro scale, meaning a large population of vehicles. These trajectories do not convey any information regarding the vehicle usage of a specific client. Consequently, they constitute a poor EDP for the forthcoming transport mission, but they serve as a good indicator of the vehicle performance. Hence, generic driving cycles like those mentioned are of great use in vehicle-to-vehicle comparisons, for determining the average energy consumption of a fleet, and for regulatory evaluations of countries and vehicle manufacturers. However, for client or transport mission-specific EDPs, the specific vehicle use is of importance as it may vary significantly from the generic driving cycles. In [25], a bus rapid transit driving cycle is developed, where vehicle log files are used to estimate the driving cycle of a bus line in heavy traffic. Using this driving cycle in EDPs shall capture the vehicle use of that specific bus line. Despite this, one cannot from this model distinguish between dense or sparse traffic, effects of weather conditions, or other factors, as merely the average dense traffic speed profile is used. It is plausible that the bus may not stop at all bus stops during nighttime, changing the speed profile. An alternative approach to driving cycles was discussed in Section 2.1, in which road information guides the generation of a trajectory. A third approach is plausible when the trajectory has already been observed. By using a Kalman filter or some other kind of signal manipulation, the higher order derivatives of position may be estimated merely from a position timeseries, outlining the trajectory generator developed in Paper B. It functions as follows: consider the vehicle to be a point in a one-dimensional space with position $s(t)$, velocity $v_x(t)$, and acceleration $a_x(t)$, all of which are continuous functions of time, hence:

$$v_x(t) = v_{\mathrm{v},x}(0) + \int_0^t a_x(t')\,\mathrm{d}t', \tag{2.22}$$

$$s_x(t) = s_{\mathrm{v},x}(0) + v_x(0)\int_0^t \mathrm{d}t' + \int_0^t \int_0^t a_x(t')\,\mathrm{d}t'\,\mathrm{d}t'. \tag{2.23}$$

By introducing the sample time ΔT, the system has the exact discrete-time solution,

$$v_{x,\,k+1} = v_{x,\,k} + \Delta T a_{x,\,k}, \tag{2.24}$$

$$s_{x,\,k+1} = s_{x,\,k} + \Delta T v_{x,\,k} + \frac{(\Delta T)^2}{2} a_{x,\,k}, \tag{2.25}$$

under the assumption that the state derivatives are piecewise constant over the time interval $(k, k+1)$ and that the initial states are known. Without any particular insights about the dynamics of the acceleration, the best approximation is to assume the state is constant, and describe the uncertainty related to this assumption using a random variable $\tilde{q}_k$. From this assumption and the equations that have been stated, a state space model,

$$\begin{bmatrix} s_{x,\,k+1} \\ v_{x,\,k+1} \\ a_{x,\,k+1} \end{bmatrix} = \begin{bmatrix} 1 & \Delta T & \frac{(\Delta T)^2}{2} \\ 0 & 1 & \Delta T \\ 0 & 0 & 1 \end{bmatrix} \begin{bmatrix} s_{x,\,k} \\ v_{x,\,k} \\ a_{x,\,k} \end{bmatrix} + \begin{bmatrix} 0 \\ 0 \\ 1 \end{bmatrix} \tilde{q}_k \tag{2.26}$$

that describes the motion of a vehicle can be formed. Notably, for all states to be observable, the requirement of measuring $s_{x,\,k}$ must be satisfied.

The Kalman filter, as described above do not convey any information about travel direction. As the odometer merely measures distance rather than position, it cannot produce negative velocity measurements. It is therefore beneficial to constrain the estimate, such that only positive velocities can be attained. This can be accomplished by projecting the estimate onto the constrained space using, for instance, the active set method. A more detailed description of how this can be performed is presented in Paper B and [26][27].

Chapter 3

Energy demand uncertainty

With vehicles becoming smarter every day, the demand for information has grown to an all-time high. In particular, uncertainties in range estimation have recently been a requested feature for the design of safeguards concerning destination attainability [28] and in solving the electric vehicle routing problem under chance constraints [16]. By now, there are numerous methods for estimating this, with the simplest and most adopted being derived from data. A common routine is to derive the uncertainty from a model output to vehicle log data comparison, with high-fidelity simulation data sometimes being used instead. With this approach, the generic model performance is rather difficult to assess as the results are only valid for the transport operations that have been considered in the comparison. Even under similar operating conditions, merely a change in travel distance will impact the EDP uncertainty, as was shown in Paper A. The issue may be addressed by estimating the uncertainty directly inside the EDP algorithm, rather than deriving it from data in hindsight. For instance, in [29], a stochastic differential equation is solved, in which the road grade is modeled by a Uhlénbeck-Ornstein process. The resulting algorithm provides an EDP uncertainty estimate considering the road topography as a stochastic variable. In [30], the EDP uncertainty under noisy reference speed measurements is investigated, utilizing an inverse dynamic model as opposed to the stochastic differential equation just mentioned. In Paper A, an observer-based EDP model is developed, addressing the EDP uncertainty by regarding the driver as a measurement. Apart from EDP uncertainty, the framework explains the uncertainty associated with vehicle speed, elevation, road grade, and tyre temperature. In contrast to the other methods mentioned, the observer-based EDP model demonstrates an easily expandable and computationally efficient format, permitting inclusion of more uncertainty sources without deteriorating the computational efficiency. However, the model is fairly complex, demanding further explanation and exemplification, for it to be understood and accepted. Hence, this Chapter presents two alter-

native methods, including the well-established *Monte Carlo method* (MCM), and the *Ensemble Kalman Filter* (EnKF), that both share similarities to the *Cubature Rauch-Tung-Streibel* (CRTSS) algorithm. In the first Section, an inverse dynamic and a dynamic model utilize the MCM to attain the EDP uncertainty arising from a stochastic reference speed, using similar methods to those developed in [30]. Likewise, the second Section introduces another method that utilizes the MCM, namely the EnKF. In contrast to the first, the EnKF utilizes the same observer-based approach as the CRTSS, having similar fundamental equations. Finally, a brief discussion of the advantages and potential enhancements of the CRTSS algorithm is presented.

3.1 Monte Carlo method

A simple yet effective method for estimating the moments of a system output variable is to utilize the Monte Carlo Method (MCM). It unfolds by repeatedly simulating the system using realizations from a random input or parameter. After the simulations, the sample mean and variance of any system variable can be calculated and studied. To use it, the random variable must be defined in a way that allows for the drawing of random samples from it, and the output variable to be studied must be of finite variance. Under these premises, the MCM can be used to transform the uncertainties of a random variable through a system, non-linear or linear, to estimate the output variable's uncertainty. Certainly, the method allows the use of complex systems and random variable dynamics, and poses no real constraint on the analysis except for the increased computational power requirements compared to a simulation of a deterministic system.

In this Section, the MCM is deployed as an intelligible instance of an EDP uncertainty estimator, which later will be shown to share similarities with the more intricate CRTSS algorithm. For this example, the minimal state vector is adopted, $x = v_x$, with one source of randomness, v_{ref}, which is deemed sufficient for the analysis taking place in this Section. Indeed, modeling of tyre temperature, weather condition uncertainty, and other relevant parameters shall increase the accuracy, but at the cost of interpretability. Motivated by the purpose of this Section, these more intricate interrelations between states are neglected, and the most rudimentary models are instead adopted. With only one state variable, the system is merely governed by Newton's second law, which for longitudinal vehicle dynamics is the sum of motion resistances F_{mr} and the control input, traction force F_{t}, which essentially is a function of the accelerator pedal angle, brake pedal angle, and the drivetrain. Generally, such a system is described with time as the independent variable, but for good reasons, is throughout of this Section expressed in the spatial domain. Building on this, the system and its homogeneous part,

which consists of air drag F_{ad}, rolling resistance F_{rr}, and hill climbing force F_{hc}, is described by the set of equations:

$$\frac{\mathrm{d}}{\mathrm{d}s}v_x = \frac{F_{\mathrm{t}} - F_{\mathrm{mr}}}{mv_x}, \qquad F_{\mathrm{mr}} = F_{\mathrm{ad}} + F_{\mathrm{rr}} + F_{\mathrm{hc}}. \tag{3.1}$$

For simplicity, the airdag model used is independent of the weather conditions, allowing the air drag force to be estimated merely by the use of frontal area A_{f}, a constant air density ρ, a constant air drag coefficient C_{D}, and the vehicle speed v_x. These simplifications not only reduce the complexity of the model but also the information requirements, which otherwise may include wind speed, wind direction, vehicle global heading, air density, vehicle side area, and vehicle combination type. Analogously, the rudimentary rolling resistance model is used, postulating that the force is proportional to the GCW. Moreover, dependencies on tyre temperature and inflation pressure are neglected, rendering the system model time-invariant, i.e, a constant proportionality coefficient can be used, commonly known as the rolling resistance coefficient C_{rr}. Owing to these considerations, the motion resistance models used are:

$$F_{\mathrm{ad}} = \frac{1}{2}A_{\mathrm{f}}\rho C_{\mathrm{D}}v_x^2, \qquad F_{\mathrm{rr}} = C_{\mathrm{rr}}mg, \qquad F_{\mathrm{hc}} = mg\sin\theta. \tag{3.2}$$

Having established the homogeneous part of the equation of motion, a control input shall be designed, viz., the traction force, i.e, modeling of the accelerator and brake pedals. This type of driver was already introduced in equation (2.8), but is here repeated for ease of reading:

$$F_{\mathrm{t,\,d}} = K_{\mathrm{p}}(v_{\mathrm{ref}} - v_x), \tag{3.3}$$

It minimizes the difference between reference speed v_{ref} and vehicle speed v_x by adopting a proportional controller with the gain K_{p}. By this, the complexity of the system dynamics is kept low, and more intricate modeling of the reference speed can be adopted in the tactical driver that was presented in Section 2.1. In essence, the tactical driver utilizes information about the transport mission, including legal speed, curvature, traffic control devices, and mission stops to produce an accurate reference speed that the operational driver can use to estimate the traction force.

Thus far, the necessary theoretical constructs, equations (3.1)-(3.3), for the MCM have been established, and the algorithm can now be presented. In Figure 3.1, a schematic diagram of an MCM based EDP algorithm is presented, in which the reference speed is the random process input. It unfolds by the tactical driver first generating an equidistant spatially resolved reference speed profile, of which each sample is arranged Δs meters apart in sequence, conveying one transport mission. Considering a single simulation i at a single point in space k, the reference

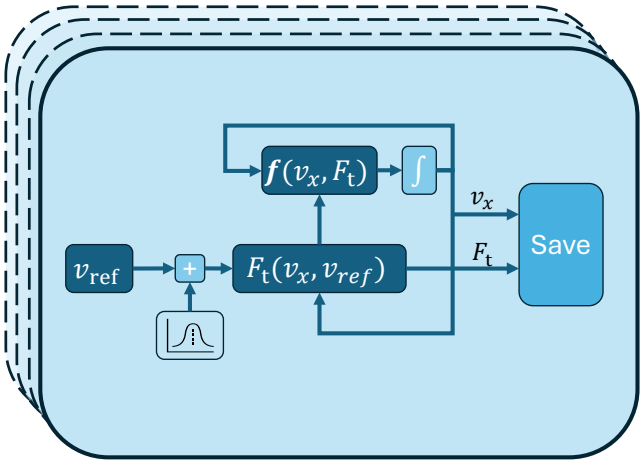

Figure 3.1: The figure is a schematic representation of how the EDP uncertainty under reference speed perturbations can be attained using MCM. By computing the sample variance over all simulations, the EDP uncertainty under reference speed perturbations may be obtained. Notably, its system description corresponds to the dynamic simulation model, though the inverse dynamic model could be handled similarly.

speed $v_{\text{ref},\,k,\,i}$ can be extracted from the input vector, and a perturbation $r_{k,\,i}$ may be generated. To avoid complex interrelations, the perturbation is assumed to be independent and identically distributed (i.i.d), such that the perturbed reference speed,

$$\tilde{v}_{\text{ref},\,k,\,i} = v_{\text{ref},\,k,\,i} + r_{k,\,i}, \qquad r_{i,\,k} \sim \mathcal{N}(0, \sigma_r^2), \tag{3.4}$$

can be expressed as a linear combination of the reference speed and the perturbation, characterized by its normal distribution. Building on $\tilde{v}_{\text{ref},\,k,\,i}$ and $v_{x,\,k,\,i}$, the traction force and motion resistances may be calculated. With the forces established, the motion can be calculated utilizing an integration method, for instance, the Euler forward method:

$$v_{x,\,k+1,\,i} = v_{x,\,k,\,i} + \Delta s \frac{F_{\text{t},\,k,\,i} - F_{\text{mr},\,k,\,i}}{m v_{x,\,k,\,i}}. \tag{3.5}$$

At this point, one step of a single simulation has been completed, meaning that the vehicle has traveled a distance Δs. Utilizing the same method repeatedly, the entire transport mission may be simulated, i.e, over all unit steps, $k \in \{0, 1, \ldots, n\}$. Meanwhile, $m + 1$ simulations with different realizations of the perturbation are conducted, comprising the second axis of each variable, $i \in \{0, 1, \ldots, m\}$. To elucidate the MCM, a single instance i represents a deterministic simulation, of which the reference speed was sampled with some particular perturbation. By repeating this simulation with new realizations of the perturbation, the variation

in system variables may be approximated by the sample variance. Notably, all parameters but the reference speed perturbation remain constant over i but may be spatially dependent over k, meaning each simulation is conducted on the same transport mission characterized by the altitude profile, reference speed, and cargo weight, all of which are spatially dependent parameters.

In [31], a similar method was developed, but by varying more parameters than just the reference speed. In that paper, the inverse dynamic model,

$$F_{\mathrm{t,\,id}} = ma_x + F_{\mathrm{mr}} \tag{3.6}$$

is utilized, as opposed to the dynamics simulation model (3.1) presented in this Section. The model has no states, and the traction force is defined as the force required to satisfy a predefined motion. Following this, the reference speed becomes a crucial parameter as the vehicle is constrained to follow it strictly, potentially requesting more power than can be delivered by the vehicle. In contrast, the dynamic simulation model permits the driver to deviate from the reference speed locally, as the force is only proportional to the difference, $\tilde{v}_{\mathrm{ref}} - v_x$, resulting in a behavior similar to a low-pass filter, under the assumption that K_p is chosen such that the system is damped. In the inverse dynamic model, there's no such filter, which makes the model more sensitive to perturbations. To quantify and prove this effect, the EDP uncertainty is computed analytically for both of the models, starting with the traction force variance of the dynamic simulation model,

$$\mathrm{Var}[F_{\mathrm{t,\,d}}] = \mathrm{Var}[K_{\mathrm{p}}(v_{\mathrm{ref}} + r - v_x)] = K_{\mathrm{p}}^2\sigma_r^2, \tag{3.7}$$

where the subscripts indicating time k and simulation i are dropped for ease of notation. By acknowledging v_{ref}, v_x, and K_{p} as deterministic variables, the traction force variance becomes proportional to the perturbation variance, simply a linear transform.

In contrast, the inverse dynamic model's variance is slightly more difficult to derive. But before delving into the variance, the acceleration must be described in terms of velocities. By assuming constant acceleration and employing the kinematic relationship, the inverse dynamic model can be expressed as:

$$F_{\mathrm{t,\,id}} = m\frac{(v_{\mathrm{ref}} + r_k)^2 - (v_{\mathrm{ref}} + r_{k+1})^2}{2\Delta s} + F_{\mathrm{mr}}, \tag{3.8}$$

where Δs is the road segment length. To further simplify the calculations, it is assumed that two consecutive road segments have the same reference speed but differ in their perturbation, giving:

$$F_{\mathrm{t,\,id}} = m\frac{(r_k^2 + 2v_{\mathrm{ref}}r_k) - (r_{k+1}^2 + 2v_{\mathrm{ref}}r_{k+1})}{2\Delta s} + F_{\mathrm{mr}}. \tag{3.9}$$

In equation (3.9), a nonlinear transformation of random variables can be identified, namely, $g(X) = X^2 + \kappa X$ with $\kappa := 2v_{\text{ref}}$ and $X = r_{k'} \sim \mathcal{N}(0, \sigma_r^2)$ for $k' \in \{k,\ k+1\}$. This introduces additional complexity into the calculations compared to the dynamic model previously derived, albeit it is not an impossible feat. Fortunately, evaluating the variance of $g(X)$ provides an immediate means to determine the traction force variance,

$$\text{Var}[F_{\text{t, id}}] = \text{Var}[\frac{m}{2\Delta s}(g(r_k) - g(r_{k+1})) + F_{\text{mr}}], \tag{3.10}$$

as it is linear in $g(X)$, assuming i.i.d perturbations. Its solution can be found through adopting the variance formula $\text{Var}[g(X)] = \mathbb{E}[g(X)^2] - (\mathbb{E}[g(X)])^2$, with each term corresponding to:

$$\mathbb{E}[g(X)] = \mathbb{E}[X^2] + \kappa\mathbb{E}[X], \tag{3.11}$$
$$\mathbb{E}[g(X)^2] = \mathbb{E}[X^4] + \kappa^2\mathbb{E}[X^2] + 2\kappa\mathbb{E}[X^3], \tag{3.12}$$

following from the linearity of the expectation operator. Moreover, assuming the perturbations are zero-mean and normally distributed allows for describing the moments by merely the variance:

$$\mathbb{E}[X] = 0, \qquad \mathbb{E}[X^2] = \sigma_r^2, \qquad \mathbb{E}[X^3] = 0, \qquad \mathbb{E}[X^4] = 3\sigma_r^4. \tag{3.13}$$

Certainly, other types of distributions may better represent reality, but that remains unexplored for now. By combining the variance formula and equations (3.11)-(3.13), the variance of $g(X)$ can be expressed as:

$$\text{Var}[g(X)] = 3\sigma_r^4 + \kappa^2\sigma_r^2 - (\sigma_r^2)^2 = 2\sigma_r^4 + \kappa^2\sigma_r^2, \tag{3.14}$$

with the perturbation variance and κ as the only parameters. Finally, by assuming deterministic motion resistance, and utilizing the i.i.d property of the perturbation, the complete traction force variance may now be expressed as:

$$\begin{aligned}\text{Var}[F_{\text{t, id}}] &= \text{Var}[m\frac{g(r_k) - g(r_{k+1})}{2\Delta s} + F_{\text{mr}}] \\ &= (\frac{m}{2\Delta s})^2(\text{Var}[g(r_k)] + \text{Var}[g(r_{k+1})]) \\ &= 2(\frac{m}{2\Delta s})^2(2\sigma_r^4 + 4v_{\text{ref}}^2\sigma_r^2) = (\frac{m}{\Delta s})^2(\sigma_r^4 + 2v_{\text{ref}}^2\sigma_r^2).\end{aligned} \tag{3.15}$$

With the variance of the dynamic and inverse dynamic models derived, it is clear how they differ, but not which is the largest. In the dynamic simulation, the traction force variance depends on the gain K_{p} and the perturbation variance, whereas the inverse dynamic model exhibits dependencies on the GCW, sampling distance, perturbation variance, and reference speed. Building on these findings,

both models are to be simulated over a transport mission to determine their variance using MCM. To do so, a transport mission in which the CRTSS algorithm performed exceptionally well is studied, anticipating that a similar outcome can be observed in the MCM. In the simulations, the parameters listed in Table 3.1 are employed, representing an arbitrary heavy vehicle. Certainly, a more precise representation of the motion resistance could have been obtained by a thorough parameter identification. However, the conclusions drawn in this Section concern other vehicles than the specific test vehicle, permitting the use of artificial vehicle parameters without deteriorating the results.

Table 3.1: Parameter values utilized in the MCM algorithm.

Parameter	Description	Value	Unit
A_f	Front area	10	m^2
ρ	Air density	1.29	$\mathrm{kg\,m}^{-3}$
C_D	Air drag coefficient	0.6	–
C_rr	Rolling resistance coefficient	0.006	–

In the comparison, energy demand is evaluated rather than the traction force, as that is the objective for the majority of this thesis. It is computed by integrating the propulsion force over distance as follows:

$$E_{n,\,i} = \eta_\mathrm{p}^{-1} \Delta s \sum_{k=0}^{n} \max(F_{\mathrm{t},\,k,\,i}, 0). \tag{3.16}$$

In equation (3.16), the max function represents the pedal arbitration function that was introduced earlier, and η_p represents the drivetrain efficiency. Notably, to compare the model output with vehicle log data, the inclusion of a drivetrain efficiency is required, owing to the vehicle's inability to measure the energy demand. Having the energy demand derived for each simulation i, the mean and variance can be computed as:

$$\mathbb{E}[E_n] = \frac{1}{m+1} \sum_{i=0}^{m} E_{n,\,i}, \qquad \mathrm{Var}[E_n] = \frac{1}{m} \sum_{i=0}^{m} (E_{n,\,i} - \mathbb{E}[E_n])^2. \tag{3.17}$$

For a schematic representation of how the complete model operates, see Figure 3.2. With the moments derived, it now only remains to compare the model's performance over the transport mission previously discussed. But before the perturbations are introduced, each model is simulated with a deterministic reference speed $\sigma_r = 0$ to verify the validity of the coming results. The results are presented in Figure 3.3, in which no significant difference between the dynamic and inverse dynamic model can be observed. With the models confirmed, the sensitivity of

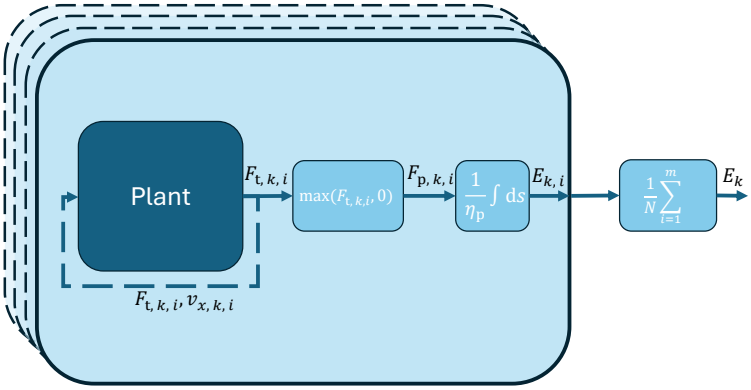

Figure 3.2: The figure is a schematic representation of how the mean energy demand can be predicted using MCM with reference speed perturbations. Here, each simulation instance computes its own energy demand, and the mean is subsequently calculated, adhering to the procedure outlined in equation (3.16)-(3.17).

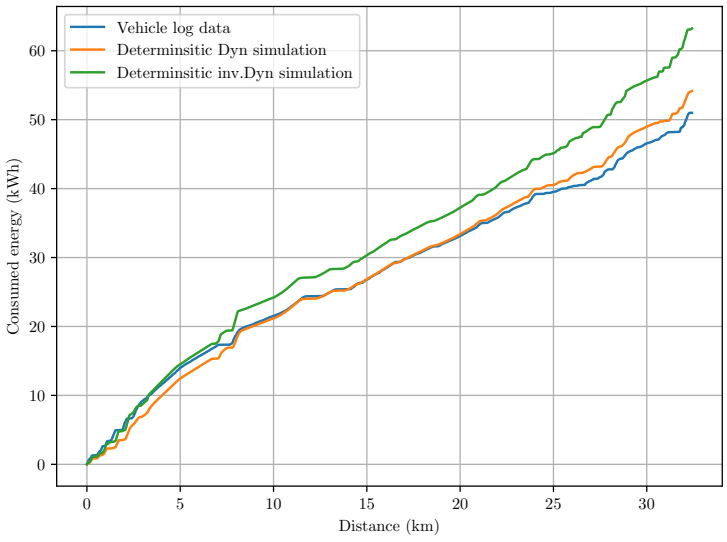

Figure 3.3: Under a specific test scenario with no perturbations, the energy demand is predicted by the dynamic simulation model (orange) and the inverse dynamic model (green). It can be concluded that both models are comparable to the vehicle log data (blue).

them concerning reference speed perturbations can now be examined. In Figure 3.4, the mean energy consumption using both models is presented over a specific transport operation under rather big perturbations $\sigma_r = 2\,\mathrm{m\,s^{-1}}$. From the figure,

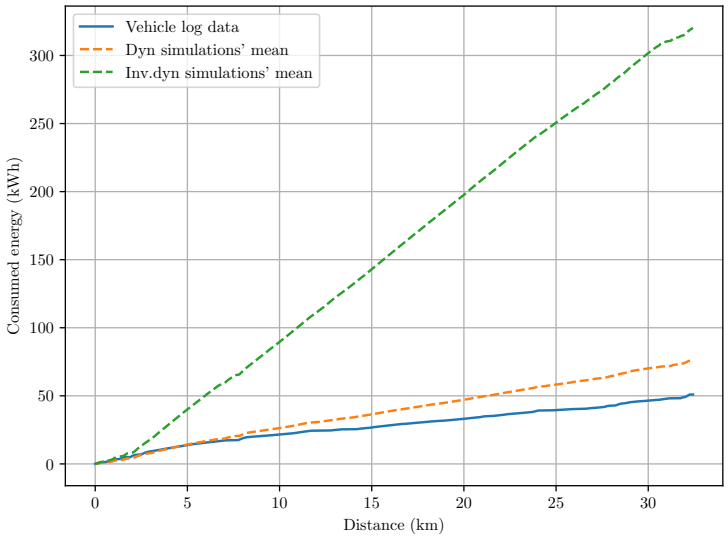

Figure 3.4: Under a specific test scenario with reference speed perturbations sampled with $\sigma_r = 2\,\mathrm{m\,s^{-1}}$, the energy demand is predicted by the dynamic simulation model (orange dashed) and the inverse dynamic model (green dashed). It can be concluded that both models are comparable to the vehicle log data (blue solid).

it can be observed that the inverse dynamic model is relatively inaccurate in its prediction, whilst the dynamic simulation model performs much better. It can also be identified that both models have their mean energy consumption increased by the introduction of the perturbation. This can be explained by the truncation that takes place in the pedal arbitration function, as was discussed briefly in Paper B.

Depending on the purpose of the study, this increase in energy demand may be undesirable. To address this, one may instead derive the EDP mean and variance from the traction force by first computing its moments:

$$\mathbb{E}[F_{\mathrm{t},\,k}] = \frac{1}{m+1}\sum_{i=0}^{m} F_{\mathrm{t},\,k,\,i}, \qquad \mathrm{Var}[F_{\mathrm{t},\,k}] = \frac{1}{m}\sum_{i=0}^{m}(F_{\mathrm{t},\,k,\,i} - \mathbb{E}[F_{\mathrm{t},\,k}])^2. \tag{3.18}$$

The random variable $F_{\mathrm{t},\,k}$, characterized by the mean and variance just derived, can now be leveraged in deriving the EDP's corresponding moments. By adopting the same procedure as is outlined in Paper A, it follows that the EDP mean and

variance can be computed as:

$$\mathbb{E}[E_n] = \eta_{\mathrm{p}}^{-1} \Delta s \sum_{k=0}^{n} \max(\mathbb{E}[F_{\mathrm{t},\,k}], 0), \quad \mathrm{Var}[E_n] = (\Delta s)^2 \eta_{\mathrm{p}}^{-2} \sum_{k=0}^{n} \mathrm{Var}[F_{\mathrm{t},\,k}]. \quad (3.19)$$

For a schematic representation of how the complete model operates, see Figure 3.5.

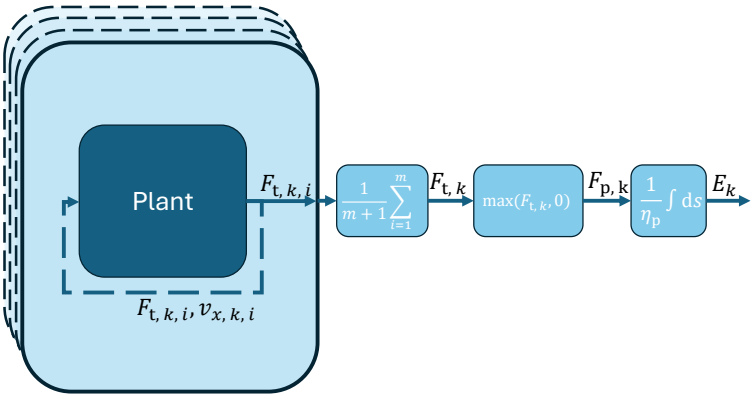

Figure 3.5: The figure is a schematic representation of how the mean energy demand can be predicted using MCM with reference speed perturbations. Here, the mean traction force is first derived, which is subsequently used to determine the mean energy demand, adhering to the procedure outlined in equation (3.18)-(3.19).

Using the formulas outlined in equation (3.19), the EDP moments can now be computed over the same transport mission that was studied previously. In Figure 3.6, the results from the dynamic simulation model are presented. The inverse dynamic counterpart is presented in Figure 3.7, in which three curves can be identified, representing the vehicle log data, the MCM-based simulation mean, and the deterministic simulation mean. Based on these figures, it can be concluded that the second definition of the mean energy demand, equation (3.18)-(3.19), is effective. The small difference in how the moments are calculated shows to have a significant impact on the resulting EDP, as can be seen when comparing Figure 3.6 and 3.7 to Figure 3.3 and 3.4.

Comparing Figure 3.6 to Figure 3.7, reveals that the inverse dynamic model exhibits significantly larger variance, indicated by the shaded area, compared to the dynamic model. In addition, the inverse dynamic mean energy demand, indicated by the dotted line, has a larger average incline than the vehicle logged data, the dynamic simulation, and the deterministic inverse dynamic simulation. Conversely, the dynamic simulation model shows few signs of being affected by the perturbations, as the expected value is similar to that of the logged vehicle and the deterministic dynamic simulation. The effect is also clear when inspecting

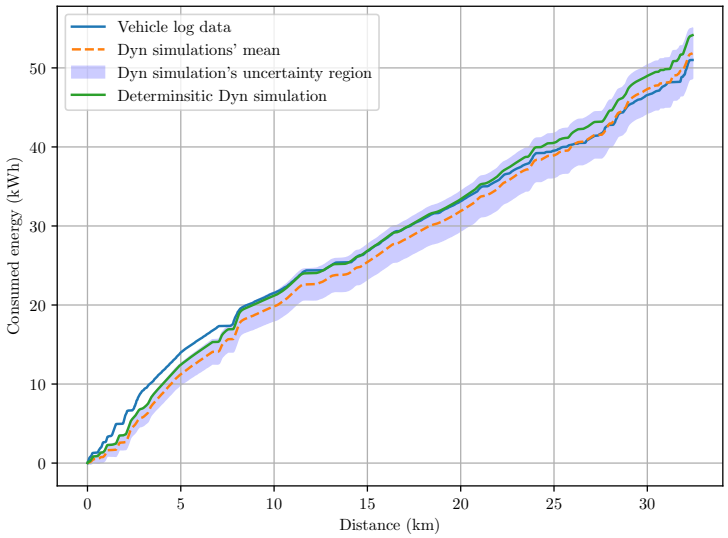

Figure 3.6: Under a specific test scenario with reference speed perturbations sampled with $\sigma_r = 2\,\mathrm{m\,s^{-1}}$, the energy demand is predicted by the dynamic simulation model. The mean energy demand (orange dashed), the deterministic simulation (green solid), and the vehicle log data are nearly aligned and mostly within the uncertainty region (blue area).

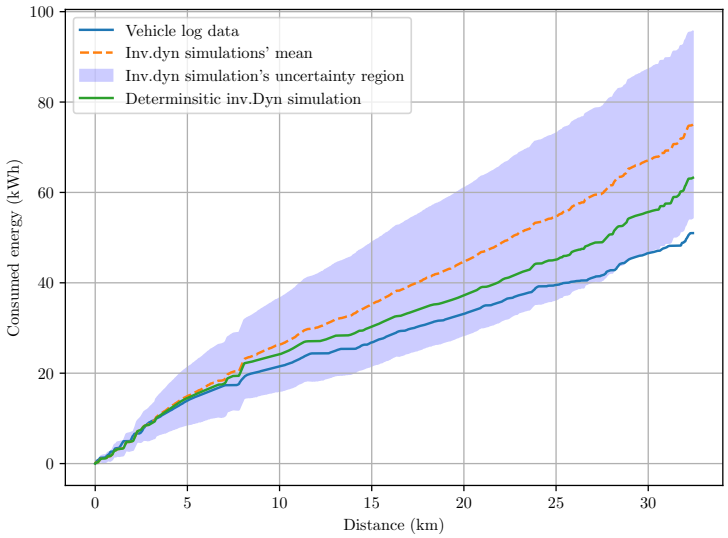

Figure 3.7: Under a specific test scenario with reference speed perturbations sampled with $\sigma_r = 2\,\mathrm{m\,s^{-1}}$, the energy demand is predicted by the inverse dynamic simulation model. The mean energy demand (orange dashed), the deterministic simulation (green solid), and the vehicle log data are mostly within the uncertainty region (blue area) but progressively diverge from each other.

the velocity profiles presented in Figure 3.8. In the figure, it is evident that the dynamic model is much more resilient to fast disturbances as its velocity profile is smoother than that of the inverse dynamic model.

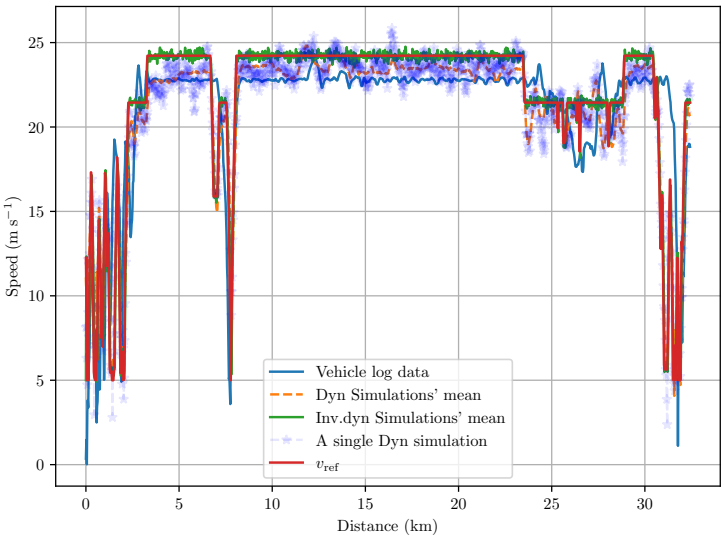

Figure 3.8: Under a specific test scenario with reference speed perturbations sampled with $\sigma_r = 2\,\mathrm{m\,s^{-1}}$, the inverse dynamic and dynamic models are both evaluated. To compare them, the longitudinal vehicle speed corresponding to: vehicle log (blue solid), dynamic simulation mean (orange dashed), the inverse dynamic simulation (green solid), a single instance of the dynamic simulation (blue star), and the original reference speed (red solid) is presented.

To conclude this Section, the reference speed sensitivity of two simulation models: the inverse dynamic and the dynamic model, was evaluated using the MCM. It was shown that the inverse dynamic model is more sensitive to perturbations concerning its mean. To mitigate this effect, an alternative approach to computing the EDP moments was developed, proving to be very effective. Finally, the models were evaluated over a transport mission, and a discussion about the results was held. In the coming Chapter, the Ensemble Kalman filter is introduced, bearing similarities with both the MCM and the CRTSS model, which is later discussed.

3.2 Ensemble Kalman Filter

Another method for estimating the moments of a system variable is the *Ensemble Kalman Filter* (EnKF). Like the MCM, the EnKF revolves around simulating a set of particles and deriving the moments from their sample distribution. Notably, this Section will employ the term particles rather than simulations, with

the fundamental distinction that particles depend on each other. Whereas conventional simulations evolve independently, the particles in this context influence one another through the Kalman gain $\mathbf{K}$, owing to it being a function of the particle sample variance [32]. Without delving into all the details of the EnKF, the evolution of each particle is determined by the Luenberger observer framework,

$$\hat{\boldsymbol{x}}_{k|k} = \hat{\boldsymbol{x}}_{k|k-1} + \mathbf{K}(y_k - \mathbf{H}\hat{\boldsymbol{x}}_{k-1|k-1}), \tag{3.20}$$

which fuse the state prediction with the measurement. This formulation is realized by treating the reference speed as a measurement, rather than an input, utilizing the same proportional driver previously presented. By rearranging the terms slightly, the measurement equation with states on one side and measurement on the other is attained:

$$v_{\text{ref}} = \frac{F_{\text{t}}}{K_{\text{p}}} + v_x + r, \qquad r \sim \mathcal{N}(0, \sigma_r^2). \tag{3.21}$$

In equation (3.21), the reference speed is the measurement generated from a tactical driver, which considers road information such as the legal speed limit, curvature, traffic control devices, and mission information. Certainly, the model cannot perfectly describe a real driver, which is why the random variable r is introduced, representing this discrepancy.

Analogously to the MCM, the motion of the vehicle is described along its longitudinal axis, in which the motion resistances, consisting of the air drag F_{ad}, the rolling resistance F_{rr}, and the hill climbing force F_{hc} act:

$$F_{\text{ad}} = \frac{1}{2} A_{\text{f}} \rho C_{\text{D}} v_x^2, \qquad F_{\text{rr}} = C_{\text{rr}} m g, \qquad F_{\text{hc}} = m g \sin\theta. \tag{3.22}$$

In contrast to previous models discussed, the EnKF is a state observer, demanding the traction force to be described as a state rather than an input. As no prior knowledge of it is attained, the most rudimentary model is adopted, that is, quasi-stationary traction force:

$$\frac{\mathrm{d}}{\mathrm{d}s} F_{\text{t}} = 0 \tag{3.23}$$

Altogether, the equations of motion may now be formed in the spatial domain:

$$\frac{\mathrm{d}}{\mathrm{d}s} v_x = \frac{F_{\text{t}} - F_{\text{mr}}}{m v_x}, \qquad F_{\text{mr}} = F_{\text{ad}} + F_{\text{rr}} + F_{\text{hc}}. \tag{3.24}$$

With the equations in place, the EnKF algorithm is now to be explained. In Figure 3.9, a flow diagram is presented, representing the underlying architecture of the algorithm. Analogously to the MCM, a reference speed sample at time k is extracted, and a perturbation is added. In parallel, the measurement equation

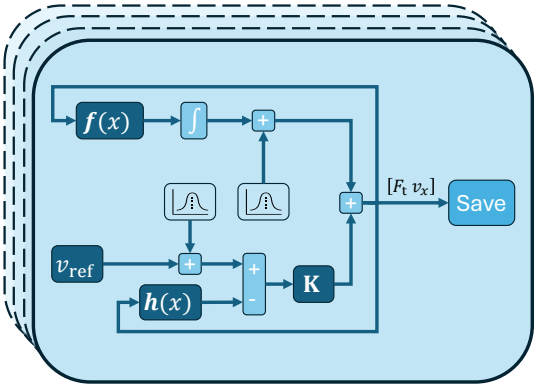

Figure 3.9: The figure is a schematic representation of an EnKF algorithm. The algorithm functions by adding a perturbation to v_{ref} and the state prediction, which is later fused with the innovation. At all times, j particles are simulated in parallel, and the sample mean and variance are calculated over the whole ensemble.

(3.21) is utilized to predict the reference speed. The difference between the two, also known as the innovation, is fed through and added to the state prediction. Synchronously to this process, a state estimate is produced by adding a perturbation to the one-step-ahead prediction $\hat{\boldsymbol{x}}_{k|k-1}$. Ultimately, the one particle estimate is obtained through the weighted sum of the state prediction and the innovation, following equation (3.20). By performing the same procedure for a set of particles $m+1$, an approximation of the expected value and the variance is attained, called the state estimate.

With the method outlined, the state variables may now be examined concerning accuracy, starting with the vehicle speed. In Figure 3.10, four curves representing the vehicle log data, EnKF state estimate, a single EnKF particle, and the reference speed are presented, all of which align decently with each other. The closest match to the vehicle log data is clearly the state estimate, both in terms of characteristics and in magnitude, with the particle following close behind. In contrast, the reference speed exhibits long periods of constant speed coupled with rapid accelerations over shorter segments.

Concerning the brake and propulsion forces, the traction force state estimate must first be transformed through a pedal arbitration function. For simplicity, the same pedal arbitration function as has been adopted previously is used, namely, mutually exclusive pedals:

$$F_{\text{p}} = \max(F_{\text{t}}, 0) \qquad F_{\text{b}} = \max(-F_{\text{t}}, 0). \tag{3.25}$$

After the transformation, two new state estimates can be presented in Figure 3.11. Here, four major brake events can be identified, two at the start and two at the end. By comparing the figure to the reference speed, it is evident that these

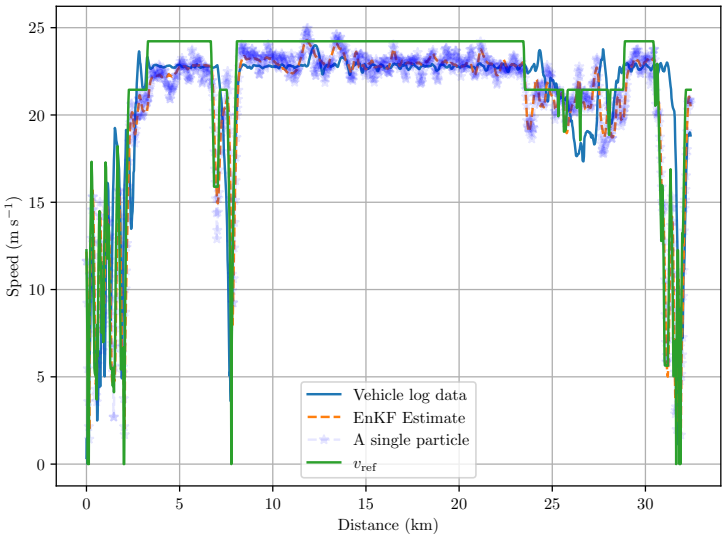

Figure 3.10: The figure contains four vehicle speed curves characterized by how they are generated. The blue solid curve represents the vehicle log data, the orange dashed the state estimate, the blue stars a single EnKF particle, and the green the reference speed.

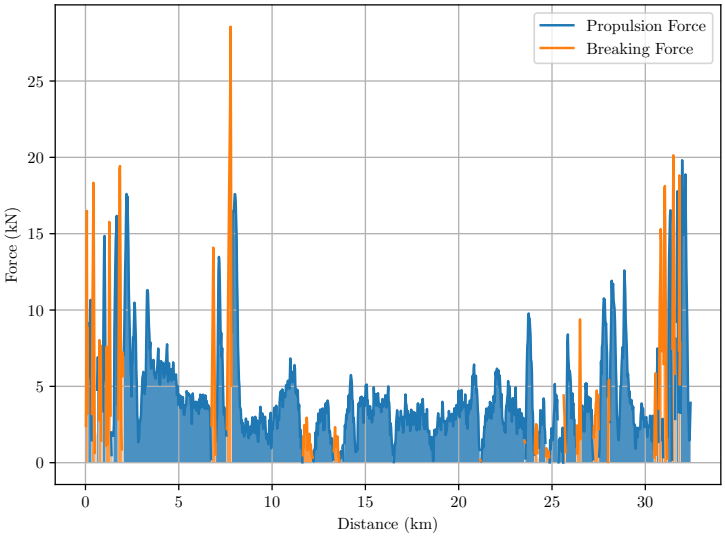

Figure 3.11: The figure represents the propulsion (blue) and braking (orange) forces that are engaged by the vehicle during a transport mission.

brake events align with Sections of rapid speed changes, in which braking shall therefore be anticipated. Apart from those, one minor brake event around 13 km can be identified, likely due to downhill driving, but that remains unconfirmed. Overall, the forces are reasonable owing to the large sections of almost constant propulsion force and minor braking action. In Figure 3.12, the energy demand's

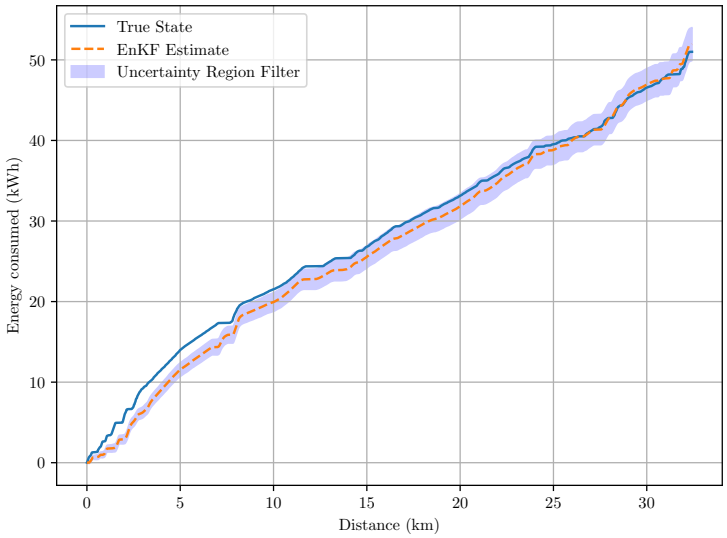

Figure 3.12: The figure represents the EDP performed by the EnKF. It presentes the true state (blue curve), the state estimate (orange dashed curve), and the uncertainty region (blue area).

first and second moment is presented along with the logged energy consumption. Here, a close match between the vehicle log data and the estimate can be observed, with the vehicle log data mostly being contained inside the uncertainty region.

3.3 Cubature Rauch Tung Striebel smoother

In this Section, an overview and discussion of the CRTSS observer is presented without delving into the details. For those, the reader is instead referred to Paper A, which presents the algorithm and results thoroughly. Because the algorithm is rather complicated, the author wishes to address potential inquiries by relating it to the more interpretable models, the MCM and EnKF. In doing so, it shall also become clear that the primary novelty of Paper A concerns the holistic architecture that has been adopted rather than the specific algorithmic choices made, such as using the CRTSS. With holistic architecture meaning adopting the observer scheme and interpreting the driver as a measurement rather than an input.

In Section 3.2, the EnKF observer was introduced, showing how the Luenberger observer scheme can be used to describe particles' evolution. Likewise, the CRTSS utilizes the same scheme but differs in how the state prediction and innovation are obtained. In Figure 3.13, a flow diagram of the algorithm is presented, which appears to be very different from the EnKF upon initial inspection, but is, in principal rather similar. Starting in the upper left corner, the CRTSS algorithm

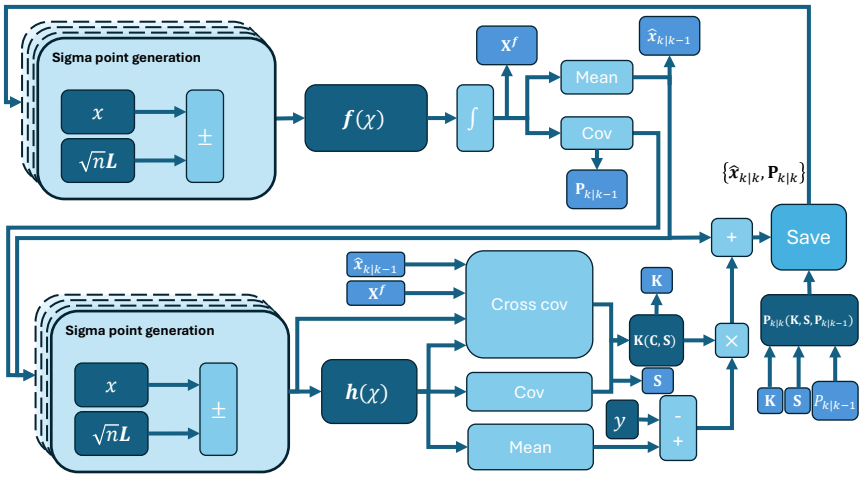

Figure 3.13: The figure is a schematic representation of an CRTSS algorithm. The algorithm functions by creating $2N$ sigmapoints which are transformed through the motion and measurement model. After each transformation, the sample mean and variance is calculated which is together used to update the state following the Luenberger equation.

initializes a set of sigmapoints, which essentially are strategically placed particles that approximate the same distribution as the EnKF perturbations did. Those particles are subsequently transformed through the motion model $f(x)$ to attain the state predictions. Likewise, a set of strategically placed particles is initialized and transformed through the measurement equation $h(x)$, which, after minor manipulation take part in the innovation together with the measurements. Finally, the state estimate is obtained from the weighted sum of the prediction and the innovation, following the Luenberger observer equation (3.20). To this end, merely minor differences between the CRTSS and EnKF algorithms can be identified, specifically, in the perturbation generation. In general, approximating a distribution by sampling is a tedious task requiring many samples to be generated before the sample distribution has converged to a satisfactory tolerance. In contrast, using the sigma point method, merely $2N$ number of particles must be generated, where N is the size of the state vector. This facilitates faster computation, but does not necessarily improve or deteriorate the performance.

Another difference between the two, following from their structure, is the traceability of individual particles. In the EnKF, each particle survives throughout the

whole transport mission, permitting the user to study single particle behavior. In contrast, the CRTSS algorithm resamples new particles at every time step, merely describing the evolution of the distribution, without capturing the dynamics describing individual particles. Certainly, the EnKF particles are not independent, following from the Kalman gain K being determined from the whole ensemble of particles, but they are traceable in time and space. However, while this property is desirable in EDPs, it is not essential, as all relevant vehicle functions ultimately rely only on the resulting distribution. Its importance shall therefore not be overstated, and attention shall instead be directed towards computational efficiency, accuracy, and robustness.

Moving on to shared benefits, the observer-based EDP algorithms can estimate other variables than energy demand, for instance, the tyre temperature, as was demonstrated in Paper A. There, an observable model was developed with five state variables and two measurement equations, which could certainly have been introduced in the EnKF as well, but was excluded motivated by simplicity. These parameters, like the tyre temperature, could potentially serve dual purposes, for instance being used in friction estimation [33] or tyre wear calculations [34]. Albeit possible, the benefits from accounting for the variance of these variable remains unknown to the author.

Chapter 4

Stochastic parameter models

In the previous Chapter, the uncertainty in EDPs was studied from the perspective of driver uncertainties. It was demonstrated that the uncertainty remains significant, even though most of the relevant information was available. The information used by these algorithms concerns the environment in which the vehicle is operating, characterized by the road, mission, and weather. For these algorithms, the energy demand is predicted over a path, with the relevant information being a function of the path itself. Hence, for the EDP algorithms to function, the transport mission must meet the necessary conditions: the route must be specified and static, see Definition 4.1.

Definition 4.1 (A specified and static route)**.** A static route is defined as a route for which all parameters are defined with maximum information. Namely, let $X(s)$ be a parameter, and $\mathcal{F}_t$ be the filtration at the time of which the EDP was conducted, and $\mathcal{F}_{t'}$ be the filtration at some later time $t < t'$. Considering a static route, the parameter is independent of the new information $\mathcal{F}_{t'} \setminus \mathcal{F}_t$ and the equality,

$$X(s)|\mathcal{F}_{t'} = X(s)|\mathcal{F}_t \tag{4.1}$$

holds. By definition, such a route must also be specified as $\mathcal{F}_{t'}$ contains all information of the traversed route.

In this context, a static route is the route that has none of its parameters altered after the start of the transport mission. The parameters may indeed change along the transport mission; however, they must be independent of the information obtained along the route. To clarify, a static route may be described with dynamic states, inputs, and parameters, but the same description shall hold once the route has been traversed. In reality, disturbances such as traffic and weather may force

the driver to diverge from the original plan, adding another source of uncertainty into the equation, but that is yet to be acknowledged by the EDP algorithms presented so far. Moreover, certain transport applications cannot provide parameter values for a desired horizon because the future is unknown to the driver, haulage, and logistics company, thereby violating the specified route assumption. Such an application may, for instance, be on-demand freight delivery trucks.

A useful mathematical toolset for describing the dynamics of these uncertain parameters is stochastic modeling. These models do not necessarily describe a specific route, but instead its probability space $(\Omega, \mathcal{F}, \mathcal{R})$, where Ω is the sample space, $\mathcal{F}$ is the filtration, and $\mathcal{P}$ is the probability measure. With these models, it is possible to describe the parameters of the transport mission without knowing them precisely. For instance, the auto-regressive model for road grade [35] or its continuous time counterpart, the Orenstein-Uhlenbeck process:

$$\mathrm{d}\theta(s) = -\alpha\theta \, \mathrm{d}s + \beta \, \mathrm{d}B(s). \tag{4.2}$$

A large collection of these models is available in the *Stochastic operating condition* (sOC) format, previously referred to as the *Stochastic operating cycle* [36] [37], which is a collection or library of stochastic models split into the categories road, mission, traffic, and weather. The sOC format describes the most relevant environment properties to energy consumption, where the focus of this Chapter will be on the Cargo weight, as it has a significant effect on the energy consumption. In Table 4.1, each model and their respective category are presented.

Table 4.1: Collection of all sOC models [36].

Parameter	Category	Independent variable
Road type	Road	Distance
Stop signs	Road	Distance
Give way signs	Road	Distance
Traffic lights	Road	Distance
Speed bumps	Road	Distance
Speed signs	Road	Distance
Topography	Road	Distance
Curviness	Road	Distance
Road roughness	Road	Distance
Temperature	Weather	Time
Relative humidity	Weather	Time
Atmospheric Pressure	Weather	Time
Precipitation	Weather	Time
Wind velocity	Weather	Time
Traffic density	Traffic	Time
Cargo Weight	Mission	Distance

4.1 Cargo weight

For vehicles in general, and especially for heavy vehicles, one of the most influential parameters concerning energy consumption is the gross combined weight (GCW), as many of the resistances are almost linearly proportional to it, including the rolling resistance, hill climbing force, and the inertial forces. Certainly, a heavier vehicle may operate with other characteristics than a light vehicle, having an impact on the inertial forces outside of the linear proportionality. Concerning the rolling resistance, a linear model is often adopted as the resistance is momentaneously, but not globally, linear with the GCW following from the tyre temperature dependency. As the tyre warms up from the accumulated heat, the rolling resistance coefficient decreases and eventually reaches a stationary temperature. The specific temperature at which the system is stable depends on, amongst others, the tyre load. Even air drag, which is formally independent of the GCW, is indirectly affected by the cargo weight, owing to it demanding certain vehicle combinations. For instance, a trailer may be attached to take parts of the cargo, resulting in a larger side area. In addition, certain cargo types are notoriously bad concerning air drag, for instance, timber due to its open trailer design. Albeit all the intricate relations, the resulting energy consumption of a heavy vehicle may be regarded as approximately linearly proportional to the GCW in most instances.

It becomes rather easy to see after factorizing the inverse dynamic model such that:

$$F_{\mathrm{t}} = F_{\mathrm{ad}} + m(C_{\mathrm{rr}}g + g\sin\theta + \frac{\mathrm{d}}{\mathrm{d}t}v_x). \tag{4.3}$$

Considering this, an accurate GCW measurement is certainly crucial for producing accurate EDPs. To understand and quantify this, methods for studying the scenario of unknown GCW are developed in this Chapter. This may be accomplished using the stochastic model developed in Paper C, but a more rudimentary approach is adopted in this thesis. Whilst the sOC model describes the vehicle-use of a specific client, the analysis performed in this thesis is performed to have a broader applicability. Before that, a post-processing method for noisy GCW measurements is developed, which could be useful for simulation studies, but also for the understanding of how GCW changes along a day of operation.

4.1.1 Gross combined weight filtering

When designing, testing, and validating the results of an EDP algorithm, it is common to compare with vehicle log data, as that is hopefully close to the ground truth. When doing so, certain vehicle log signals may be used as information to the EDP algorithm, for instance, the GCW log. This signal is, in practice, not available to the EDP algorithm as the prediction must be made before the transport mission has started, but may be used in the development phase. In the real implementation, the cargo weight must be known from weighing the container or the cargo. In this thesis, the GCW estimate for a heavy vehicle similar to Figure 2.3 with leaf spring suspension is used, which unfortunately is rather noisy. Hence, a method for GCW smoothening is developed, revolving around a method called thresholding, commonly used in image processing. It divides data points into clusters of certain characteristics, which will later be covered. To guide the choices made, the following set of assumptions was identified as reasonable in discussions with experts:

I. **GCW is constant during driving.** In almost all physically-based EDP algorithms, a trivial yet crucial model assumption is adopted. It states that the GCW is constant during driving, and that a change in GCW can only be observed when the vehicle is at a standstill. In reality, minor changes in the GCW may be observed due to the burning of fuels, rainwater accumulation, and spillage of cargo, but that is often neglected as the impact on the energy consumption is not noticeable. The first model assumption is, therefore, constant GCW during driving, allowing the simplification of Newton's equation to:

$$\frac{\mathrm{d}}{\mathrm{d}t}(mv) = m\frac{\mathrm{d}v}{\mathrm{d}t}. \tag{4.4}$$

II. **GCW can be characterized.** For instance, a rigid truck is characterized by two distinct modes: loaded and empty. In contrast, a trailer has three modes: empty, loaded, or detached. A rigid truck with a trailer therefore has six modes.

III. **The modes follow a discrete-time Markov chain.** A change in GCW may only be recorded by transitioning between two modes, of which the transition probability only depends on the current mode. This assumption neglects the possibility of unloading parts of the goods.

IV. **The transition event probability follows the Markov property.** The probability of a transition event is fully described by the current mode. This means that the distance traveled before a change in GCW, depends and depends only on the current mode. This assumption is not required for the GCW filter presented here, but is relevant for the stochastic model derived in Paper C.

From a vehicle log file, an ordered set of GCW and boolean trailer connected (TC) measurements is obtained. On this data, a thresholding filter shall be deployed to cluster the data into the six modes outlined in assumption II. This task is rather difficult, as it is often non-trivial to design these thresholds. To start, the original dataset is therefore split into two sets based on the TC signal, where S_1 and S_2 correspond to the trailer being detached and attached, respectively. In S_1, two modes are easily distinguished: an empty truck without a trailer (Empty) and a loaded truck without a trailer (Loaded). In contrast, identifying the modes of S_2 is rather difficult, as it can exhibit four modes corresponding to: a loaded or empty truck with a loaded or empty trailer. With no other option, the set of modes is therefore reduced such that the three modes: 1. loaded truck and empty trailer, 2. empty truck and loaded trailer, 3. loaded truck and loaded trailer, all are contained in the same mode denoted Loaded-T. This means that the fourth mode corresponds to an empty truck with an empty trailer (Empty-T).

Building on these modes, the threshold filter can now be introduced. Assuming that the rigid truck is lighter than 20 tonnes, and that a tare trailer weighs 7 tonnes, the following thresholds may be formed:

$$L(TC) = \begin{cases} 27, & \text{if TC} \\ 20, & \text{Otherwise.} \end{cases} \tag{4.5}$$

Based on these thresholds and the knowledge of the trailer being attached, each

GCW measurement x may be placed in one of the four clusters:

$$f(X_t) = \begin{cases} \text{Empty}, & \text{if } x \leq L(False) \\ \text{Loaded}, & \text{if } x \geq L(False) \\ \text{Empty-T}, & \text{if } x \leq L(True) \\ \text{Loaded-T}, & \text{if } x \geq L(True) \end{cases}. \tag{4.6}$$

To visualize and exemplify how the threshold filter functions, it is deployed on an arbitrary vehicle logfile with the result shown in Figure 4.1. Here, the modes and GCW are plotted against distance, showing how they both evolve in relation to each other. Notably, in the transitions from Loaded-T to Empty-T, the vehicle

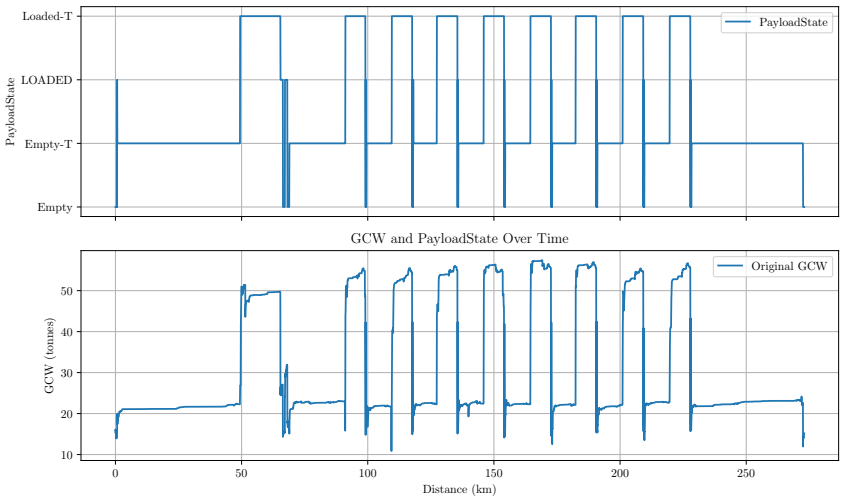

Figure 4.1: The figure consists of two subfigures sharing the same x-axis, distance. The upper subfigure represents the mode in which the truck operate and the lower displays the GCW.

seems to undergo a set of rapid transitions. To avoid those, a mode smoother is deployed, described in Definition 4.2.

Definition 4.2 (Mode smoother)**.** Let $X = \{x_0,\ x_1,\ \ldots,\ x_T\}$ be a ordered sequence of categorical labels, where $x_i \in \mathcal{L}$ and $\mathcal{L} = \{\text{Empty},\ \text{Empty} - \text{T},\ \text{Loaded},\ \text{Loaded} - \text{T}\}$ is the set of possible labels. Then the function $f : X \to \mathbb{N}^n$ returns a sequence $Y = \{y_1,\ y_2,\ \ldots,\ y_n\}$, where each y_i denotes the number of consecutive occurrences of a certain label. For all $y_i < k$, change the label of its corresponding X:s to that in y_{i-1}.

After deploying the smoother, the GCW is finally categorized. The resulting modes, is presented in Figure 4.2, in which Filtered PayloadState (orange) correspond the the new and smooth catagorization, and the Original PayloadState

represent the labeling presented in Figure 4.1. It shows that the smoother has effectively captured the major events in which the GCW changes, referred to as mission stops in this thesis. With the categorization established, the raw GCW

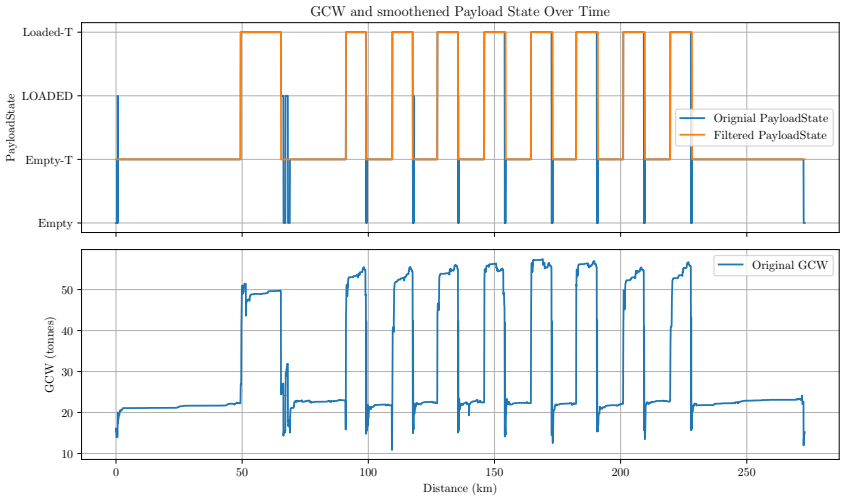

Figure 4.2: The figure consists of two subfigures sharing the same x-axis, distance. The upper subfigure represents the mode in which the truck operates, and the lower displays the GCW. Concerning the modes, two lines are presented: the original modes (blue) and the filtered modes (orange).

signal can now be smoothed. This is achieved by replacing the GCW over each sequence of contiguous modes, i.e., intervals during which the mode remains constant, with the median GCW over that same sequence. The resulting smoothened GCW is presented in Figure 4.3, which exhibits long sequences of constant GCW in between mode changes, i.e., pickup or delivery.

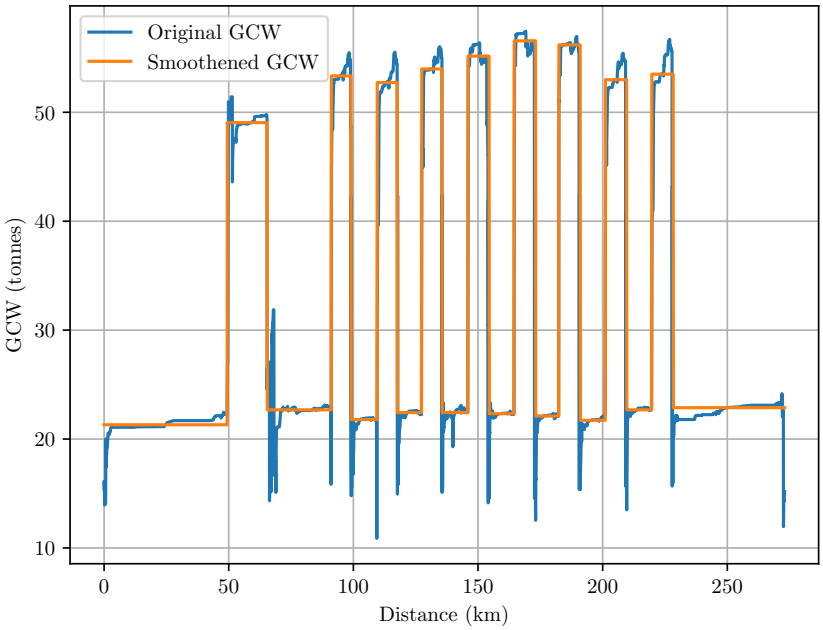

Figure 4.3: The figure consists of two curves, the original GCW measurement (blue) and the smoothed GCW estimate (orange). By visual inspection, the smoothened GCW estimate is effective in handling outliers and retaining a constant value.

4.1.2 Stochastic GCW model

The GCW smoother just described operates with full information, i.e it is aware of the past, the current, and the future GCW at any time. This acausal way of smoothening the data is what allows us to find a GCW estimate that is part-wise constant and accurate. However, due to the acausal behavior, the model cannot be used in a real-time application without modifications. Instead, the model shall be used for post-processing and analysis. One interesting aspect of the model is that it allows for building and introducing a stochastic GCW model. To avoid repetition, merely a brief explanation of this sOC model is presented in this thesis, and the curious reader is instead referred to Paper C, in which all the details are disclosed.

In short, the sOC model is characterized by its transition probabilities, transition intensities, and mode-specific distributions. Following from assumption IV, the transition probabilities between modes depend solely on the current mode, allowing the mode-switching dynamics to be represented as a Markov chain. The timing of transitions is modeled using a Poisson point process, in which the transition intensity specifies the likelihood of a transition event occurring. Finally, the distribution of the GCW within each mode is represented by a normal distribution, which was shown in Paper C to provide an adequate empirical approximation for the given vehicle-use that was studied.

4.2 Uncertainty analysis

In this Section, the same transport mission that was used in Section 3 is chosen to demonstrate the added uncertainty from not knowing the GCW. Here, 46 simulation instances are independently evolved where the vehicle operates under constant GCW. In the first simulation instance, the vehicle operated with a GCW of 15 tonnes and in the last with a GCW of 60 tonnes, with each consecutive simulation instance having its GCW increased by a tonne. To make this analysis comparable to what has previously been discussed, the same parameters and model outlined in Section 3.1 regarding the deterministic inverse dynamic simulation are adopted.

Building on this, the resulting uncertainty following from not knowing the GCW is demonstrated in Figure 4.4. Examination of the terminal simulation values reveals that the upper curve attains a magnitude of merely 2.6 times that of the lower curve, even though their GCW differ by a factor of 4. This result is not surprising, as aerodynamic drag remains unaffected by vehicle mass in these simulations. Importantly, the factor 2.6 shall not be interpreted as universally applicable, owing to its dependence on the vehicle type, its operating environment, and the driver's behavior. For instance, imagine a vehicle traveling down a hill.

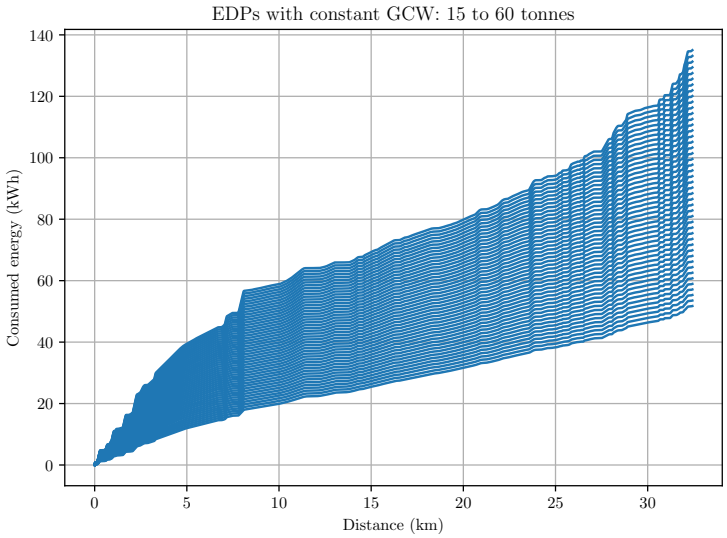

Figure 4.4: The figure represents several EDPs performed under varying GCW. Here, the bottom curve represents the transport mission characterized by a GCW of 15 tonnes whilst the upper was simulated with a GCW of 60 tonnes. Each consecutive curve is produced with a difference in GCW corresponding to a tonne.

With enough slope, the resulting EDPs would be identical, independently of the GCW, as they all would predict the energy demand to be zero. Nevertheless, under the conditions in which this experiment was conducted, the importance of accurate GCW observations for EDPs cannot be overstated. The experiment also indicates that the EDP is approximately linearly proportional to GCW, as was proposed by Section 4.1. This statement is likewise subject to discussion because, as with the factor 2.6, it depends on the driver, the vehicle, and the environment. However, it appears to be largely valid under the conditions of this experiment.

To summarize this Chapter, it was shown how one may reduce the errors in post-processing simulations by smoothening the GCW log files following the procedure outlined in Section 4.1.1. Furthermore, the sOC model for cargo weight was briefly discussed without delving into the details. Finally, the sensitivity of GCW on EDPs was studied through repeated simulations of the same transport mission but under different GCWs. By this simple simulation experiment, it becomes obvious that the cargo weight is instrumental to making accurate EDPs. In the forthcoming Chapter, the contents introduced thus far are discussed in relation to the research questions.

Chapter 5

Conclusion and future work

This thesis posed three distinct research questions, describing problems related to: **modeling**, **uncertainty**, and **abscence of observations**. The first focuses on the simplifications and assumptions often adopted by EDP algorithms, the second concerns describing uncertainties and their effect on the estimate, and the last investigates the uncertainty coupled with EDPs on an undefined mission, e.g. without GCW measurements. Together, these questions convey the importance of accounting for uncertainties in EDPs and how they propagate through the different estimation methods.

Concerning **modeling**, several models have been introduced in this thesis, including those describing the vehicle and its motion resistances in Chapter 2. From the outset, the uni-wheel vehicle was adopted, primarily due to the difficulty of predicting axle load distribution. This simplification is, to the best of the author's knowledge, always adopted by EDP algorithms, thereby precluding the possibility of estimating wheel-independent rolling resistance and tyre temperature. The field of EDPs may therefore benefit from further research into the design and development of an axle load distribution prediction model. Concerning the different types of motion resistances, it was argued that the suspension losses, cornering resistance, and tyre scrubbing can be neglected for the transport operations considered in this thesis. Albeit it is advisable to acknowledge them in other types of transport operations, e.g., urban distribution. Hence, in the design and development of a robust and generic EDP algorithm that intends to accommodate diverse operational conditions, these effects must be accounted for. Another aspect of EDPs is the availability of information and how that impacts the set of methods to choose from. In Chapter 2, a trajectory generation algorithm is presented, which was developed in Paper B. There, speedometer and odometer measurements were manipulated to obtain an acceleration profile. Notably, this approach is only valid for already traversed routes, either by the vehicle and driver themselves or by similar ones, as it requires vehicle log data. In contrast, the EDP

models presented in Chapter 3 and Paper A rely exclusively on exogenous parameters and shall in theory function on all roads, even virtual ones, owing to its vehicle log data independence. For most applications, this property is desirable as it essentially allows the algorithm to predict the energy demand on all mapped roads, which would otherwise require a considerable amount of vehicle logging to account for different vehicle types and drivers. However, in operational contexts where road data are absent, and vehicle log data constitute the sole information source, the preferred choice of estimation method is the one outlined in Paper B, specifically the trajectory generation algorithm. Clearly, all methods developed in this thesis may utilize the vehicle logged speed and are not exclusive to the inverse dynamic model presented in Paper B.

The second research question concerns how **Uncertainty** can be accounted for and estimated in an EDP algorithm. In Chapter 3, three types of estimation methods were discussed, namely: MCM, EnKF, and CRTSS, along with three different approaches to physics-based EDPs: inverse dynamic, dynamic, and the Luenberger observer. There, uncertainties in the reference speed are propagated through the vehicle model to assess their effect on energy demand. This has previously been performed using MCM, having the adverse effect of high computational complexity. It was also demonstrated that employing the MCM increases the mean energy consumption, following from random variables being transformed through non-linear convex functions. Fortunately, the observer-based models (EnKF and CRTSS) demonstrated to be rather resistant to reference speed perturbations, whilst still providing an informative uncertainty estimate. Another aspect to consider is the benefits associated with the framework developed in Paper A. Using it permits further inclusion of uncertainties, for instance, from wind and traffic, which to this day have been considered deterministic. Finally, Chapter 4 introduced a gross combined weight filter, which, although not directly addressing any EDP-related problem, serves as a valuable instrument for model validation and for assessing the performance of EDP algorithms.

The last research question addresses the problems related to **absence of observations**. The question primarily concerns vehicle cargo weight, but is not necessarily limited to that. Consider the earlier discussion on data availability, in which vehicle log data is replaced by road information through the use of a tactical driver. There, a supplementary source of data was identified, permitting EDPs to be conducted using customary methods. In contrast, parameters like the cargo weight have no alternative source of information, therefore requiring another approach. For this reason, Paper C undertook the challenge of developing a stochastic model of cargo weight. The model unfolds by describing the most probable cargo weight rather than determining it, certainly inducing uncertainties into the EDP, albeit those being smaller than any other assumption that could have been made. In Section 4.2, the GCW sensitivity of an inverse dynamic

model was studied, showing how crucial the measurement is to the EDP. Further work on this subject could be conducted, especially delving into how qualitative information could be used to reduce the uncertainty. For instance, quantifying the affect of knowing the pick-up delivery locations or understanding the type of cargo that is to be handled.

Bibliography

[1] International Energy Agency, "Global ev outlook 2025: Expanding sales in diverse markets," International Energy Agency, Tech. Rep., 2025. [Online]. Available: www.iea.org

[2] International Energy Agency, "Electric truck sales by region," 4 2025. [Online]. Available: https://www.iea.org/data-and-statistics/charts/electric-truck-sales-by-region-2016-2024

[3] H. Liimatainen, O. van Vliet, and D. Aplyn, "The potential of electric trucks – an international commodity-level analysis," *Applied Energy*, vol. 236, pp. 804–814, 2 2019.

[4] Regional Electrified Logistics (REEL), "Case overview report," CLOSER at Lindholmen Science Park AB, Tech. Rep., 12 2023. [Online]. Available: https://closer.lindholmen.se/projekt/reel

[5] R. Al-dal'ain and D. Celebi, "Planning a mixed fleet of electric and conventional vehicles for urban freight with routing and replacement considerations," *Sustainable Cities and Society*, vol. 73, 10 2021.

[6] European Commission, "Commission report under article 12(3) of regulation (eu) 2019/631 on the evolution of the real-world CO_2 emissions gap for passenger cars and light commercial vehicles and containing the anonymised and aggregated real-world datasets referred to in article 12 of commission implementing regulation (eu) 2021/392," European Commission, Brussels, Tech. Rep., 3 2024. [Online]. Available: https://www.eea.europa.eu/data-and-maps/data/data-viewers/greenhouse-gases-viewer

[7] United Nations, "Climate justice," 2019, accessed: 2026-02-08. [Online]. Available: https://www.un.org/sustainabledevelopment/blog/2019/05/climate-justice/

[8] European Parliament and Council of the European Union, "Regulation (eu) 2019/1242: Setting CO_2 emission performance standards for new heavy-duty vehicles," 2019.

[9] S. Särkkä, *BAYESIAN FILTERING AND SMOOTHING*. Cambridge University Press, 2013, vol. 3. [Online]. Available: https://users.aalto.fi/~ssarkka/pub/cup_book_online_20131111.pdf

[10] F. Klebaner, *Introduction to Stochastic Calculus with Applications*, 3rd ed. Imperial College Press, 2012.

[11] S. Hunt, A. Odhams, R. Roebuck, and D. Cebon, "Parameter measurement for heavy-vehicle fuel consumption modelling," *Proceedings of the Institution of Mechanical Engineers, Part D: Journal of Automobile Engineering*, vol. 225, pp. 567–589, 2011.

[12] J. Wahlström and L. Eriksson, "Modelling diesel engines with a variable-geometry turbocharger and exhaust gas recirculation by optimization of model parameters for capturing non-linear system dynamics," *Proceedings of the Institution of Mechanical Engineers, Part D: Journal of Automobile Engineering*, vol. 225, pp. 960–986, 2011.

[13] C. Moure, M. Arroyos, and M. Mammetti, "Range estimator for electric vehicles," *2013 World Electric Vehicle Symposium and Exhibition (EVS27*, 2014.

[14] D. Corona and B. De Schutter, "Adaptive cruise control for a smart car: A comparison benchmark for mpc-pwa control methods," *IEEE Transactions on Control Systems Technology*, vol. 16, pp. 365–372, 2008.

[15] R. Basso, B. Kulcsár, B. Egardt, P. Lindroth, and I. Sanchez-Diaz, "Energy consumption estimation integrated into the electric vehicle routing problem," *Transportation Research Part D: Transport and Environment*, vol. 69, pp. 141–167, 4 2019.

[16] R. Basso, B. Kulcsár, and I. Sanchez-Diaz, "Electric vehicle routing problem with machine learning for energy prediction," *Transportation Research Part B: Methodological*, vol. 145, pp. 24–55, 2021.

[17] C. Beckers, I. Besselink, and H. Nijmeijer, "Quantification of energy losses in suspension dampers and its effects on rolling resistance," *Vehicle System Dynamics*, vol. 21, 4 2025.

[18] A. Beckers, C. Beckers, P. Mentink, I. Besselink, and S. Wilkins, "A modular model for determining cornering resistance of heavy-duty vehicles," in *2024 IEEE Vehicle Power and Propulsion Conference (VPPC)*, 2024.

[19] H. Aldhufairi and O. Olatunbosun, "Developments in tyre design for lower rolling resistance: A state of the art review," *Proceedings of the Institution of Mechanical Engineers, Part D: Journal of Automobile Engineering*, vol. 232, pp. 1865–1882, 2018.

[20] L. Ydrefors, M. Hjort, S. Kharrazi, J. Jerrelind, and A. Stensson Trigell, "Rolling resistance and its relation to operating conditions: A literature review," *Proceedings of the Institution of Mechanical Engineers, Part D: Journal of Automobile Engineering*, vol. 235, pp. 2931–2948, 2021.

[21] J. Hyttinen, M. Ussner, R. Österlöf, J. Jerrelind, and L. Drugge, "Truck tyre transient rolling resistance and temperature at varying vehicle velocities - measurements and simulations," *Polymer Testing*, vol. 122, 3 2023.

[22] M. Askerdal, J. Fredriksson, and L. Laine, "Development of simplified air drag models including crosswinds for commercial heavy vehicle combinations," *Vehicle System Dynamics*, vol. 62, p. 1085–1102, 2023.

[23] United Nations Economic Commission for Europe (UNECE), "Global technical regulation no. 15: Worldwide harmonized light vehicles test procedure," United Nations Economic Commission for Europe, Geneva, Tech. Rep. ECE/TRANS/180/Add.15, 2014. [Online]. Available: https://unece.org/

[24] European Commission, "Commission regulation (eu) 2017/2400 implementing regulation (ec) no 595/2009 of the european parliament and of the council as regards the determination of the CO_2 emissions and fuel consumption of heavy-duty vehicles and amending directive 2007/46/ec of the european parliament and of the council and commission regulation (eu) no 582/2011," 12 2017.

[25] H. Kaymaz, H. Korkmaz, and H. Erdal, "Development of a driving cycle for istanbul bus rapid transit based on real-world data using stratified sampling method," *Transportation Research Part D: Transport and Environment*, vol. 75, pp. 123–135, 10 2019.

[26] G. Nachi and R. Hauser, "Kalman filtering with equality and inequality state constraints," Oxford University Computing Laboratory, Numerical Analysis Group, Tech. Rep. Report No. 07/18, 2008.

[27] V. Sircoulomb, G. Hoblos, H. Chafouk, and J. Ragot, "State estimation under nonlinear state inequality constraints . a tracking application," in *16th Mediterranean Conference on Control and Automation*. IEEE, 6 2008, pp. 1669–1674.

[28] S. Scheubner, A. Thorgeirsson, M. Vaillant, and F. Gauterin, "A stochastic range estimation algorithm for electric vehicles using traffic phase classification," *IEEE Transactions on Vehicular Technology*, vol. 68, pp. 6414–6428, 2019.

[29] L. Romano, K. Podgórski, C. Emvin, P. Johannesson, J. Fredriksson, and F. Bruzelius, "A stochastic theory of longitudinal dynamics and energy consumption of road vehicles," *IEEE Transactions on Intelligent Vehicles*, vol. 10, no. 3, pp. 1820–1840, 2025.

[30] S. Sautermeister, M. Falk, B. Baker, F. Gauterin, and M. Vaillant, "Influence of measurement and prediction uncertainties on range estimation for electric vehicles," *IEEE Transactions on Intelligent Transportation Systems*, vol. 19, pp. 2615–2626, 11 2018.

[31] C. Fiori, V. MARZANO, V. Punzo, and M. Montanino, "Energy consumption modeling in presence of uncertainty," *IEEE Transactions on Intelligent Transportation Systems*, vol. 22, pp. 6330–6341, 5 2021.

[32] C. Johns and J. Mandel, "A two-stage ensemble kalman filter for smooth data assimilation," *Environmental and Ecological Statistics*, vol. 15, pp. 101–110, 9 2008.

[33] A. Savkoor, "On the friction of rubber," *Wear*, vol. 8, no. 3, pp. 222–237, 1965.

[34] F. Braghin, F. Cheli, S. Melzi, and F. Resta, "Tyre wear model: Validation and sensitivity analysis," *Meccanica*, vol. 41, pp. 143–156, 4 2006.

[35] P. Johannesson, K. Podgórski, and I. Rychlik, "Laplace distribution models for road topography and roughness," *International Journal of Vehicle Performance*, vol. 3, pp. 224–258, 2017.

[36] L. Romano, "The operating cycle representation of road transport missions," Doctoral thesis, Chalmers University of Technology, Gothenburg, Sweden, 2023.

[37] P. Pettersson, "Operating cycle representations for road vehicles," Doctoral thesis, Chalmers University of Technology, Gothenburg, Sweden, 2019.